Journal of Hydrology: Regional Studies 57 (2025) 102129

Contents lists available at ScienceDirect

Journal of Hydrology: Regional Studies

journal homepage: www.elsevier.com/locate/ejrh

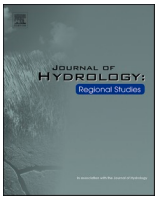

Permanent aquifer storage loss from long-term groundwater withdrawal: A case study of subsidence in Bandung (Indonesia)

Michelle Rygus [a,*], Marco Bianchi [b], Alessandro Novellino [b], Ekbal Hussain [b], Ahmad Taufiq [c], Steven Reinaldo Rusli [d], Dwi Sarah [e], Claudia Meisina [a]

[a] Department of Earth and Environmental Sciences, University of Pavia, Pavia, Italy
[b] British Geological Survey, Keyworth, Nottingham NG12 5GG, United Kingdom
[c] Center of Groundwater, Ministry of Public Work and Housing, Bandung, Indonesia
[d] Civil Engineering Department, Faculty of Engineering, Parahyangan Catholic University, Bandung, Indonesia
[e] Research Center for Geological Disaster, National Research and Innovation Agency (BRIN), Bandung, Indonesia

ARTICLE INFO

Keywords:
Groundwater overexploitation
Numerical modelling
InSAR

ABSTRACT

Study Region: In this study, the focus is on the Bandung groundwater basin in Indonesia, where industrial groundwater exploitation has led to declining groundwater levels and consequent land subsidence.

Study Focus: A highly parameterized three-dimensional hydro-geomechanical model was developed for the Bandung groundwater basin. The region faces challenges due to scarce hydrogeological data, necessitating the use of satellite-based Interferometric Synthetic Aperture Radar (InSAR) techniques to supplement the parameterization of numerical groundwater models. By calibrating the model against InSAR-derived land displacement measurements, the study addressed the lack of detailed historical pumping data and estimated past groundwater extraction volumes. The model was also used to forecast future subsidence and evaluate aquifer storage changes until 2050 under various pumping scenarios. Our study is one of the first examples of using satellite data with geomechanical models to constrain groundwater extraction rates and emphasises the importance of remote sensing data in groundwater resource management, and the irreversible impact of unsustainable groundwater extraction, which has implications for long term water security.

New Hydrological Insights for the Region: The study found that continued industrial groundwater extraction has resulted in permanent aquifer storage loss, with significant implications for long-term water security. Our simulated subsidence rates peaked at 16.4 cm/yr over the 1950–2020 period, with a maximum cumulative subsidence of 6.9 m. Continued industrial groundwater extraction, primarily from the deeper, confined aquifer, has resulted in permanent aquifer storage loss totalling 7.2 km^3. Our model projections indicate that subsidence will persist, with continued industrial extraction potentially leading to up to 5.6 m of additional subsidence and 11.1 km^3 of aquifer storage loss by 2050. Reducing industrial groundwater use by 30 % could slightly reduce further subsidence (5.0 m) and aquifer storage loss (9.2 km^3) by 2050.

* Corresponding author.
E-mail address: michelle.rygus01@universitadipavia.it (M. Rygus).

https://doi.org/10.1016/j.ejrh.2024.102129
Received 16 May 2024; Received in revised form 9 September 2024; Accepted 8 December 2024
Available online 24 December 2024

1. Introduction

Groundwater is a critical resource that plays an important role in sustaining water supplies. However, escalating trends of urbanisation and industrialisation worldwide have resulted in unsustainable groundwater exploitation of approximately 20 % of aquifers globally (Gleeson et al., 2012). In addition to the risks associated with resource scarcity, prolonged over-extraction of groundwater can lead to compaction of aquifer systems and surface settlement known as land subsidence (Davydzenka et al., 2024). Land subsidence is a geological hazard that can cause significant and recurrent damages to infrastructure, increasing the risks of flooding and water contamination, and can permanently reduce the storage capacity of aquifer systems (Guzy and Malinowska, 2020; Herrera-García et al., 2021).

The impacts of groundwater-related subsidence are generally simulated with numerical models to better understand the phenomenon and to assist in deriving sustainable groundwater management strategies (Hunt and Zheng, 2012). Crucial to the development of these models are the availability and accessibility of detailed data on subsurface conditions, ensuring representation of physical subsurface properties. The efficacy of such models is often compromised by poor data availability, uncertain conceptual frameworks, and poorly constrained parameterization (Doherty and Simmons, 2013). Traditional groundwater monitoring approaches primarily involve point-scale in-situ well data, and in many areas of the world these data are both spatially and temporally scarce and unable to adequately represent the dynamic behaviour of groundwater flow and land subsidence. Incorporating Interferometric Synthetic Aperture (InSAR) techniques can supplement point-based subsidence monitoring with a higher spatial coverage and temporal resolution (Ohenhen et al., 2024). Spaceborne InSAR exploits radar observations to measure surface deformation with millimetric precision (Sadeghi et al., 2021). Combining InSAR data with groundwater modelling makes it possible to improve the understanding of aquifer system's dynamics (Orellana et al., 2023; Bockstiegel et al., 2023). Until now, only a handful of studies, such as those conducted in Las Vegas Valley (USA) (Burbey and Zhang, 2015), Firenze-Prato-Pistoia (Italy) (Ceccatelli et al., 2021), and Semarang City (Indonesia) (Lo et al., 2022), have used the continuous spatial data offered by InSAR to augment localised field measurements and to calibrate or validate parameters for hydromechanical models dealing with the compaction of aquifer systems. The integration of InSAR-derived surface deformation measurements with numerical models enables investigations into the subsurface hydrodynamic behaviour, which facilitates predictions of groundwater-induced subsidence, and provides a way to assess long-term aquifer sustainability (Hoffmann et al., 2001; Ezquerro et al., 2017) which is key information especially in rapidly growing cities.

This study focuses on the Bandung groundwater basin located in West Java, Indonesia, which has been facing long-term and significant groundwater-related land subsidence issues, largely attributed to intense urbanisation and excessive groundwater extraction. While previous works have established numerical models to simulate groundwater flow in the Bandung Basin (Taufiq et al., 2018; Rusli et al., 2023a), none of the models have simulated groundwater extraction-induced land subsidence in this region. Furthermore, the most recent model (Rusli et al., 2023a) was not calibrated using transient data due to the lack of reliable groundwater level measurements. Incorporating temporal data to constrain the transient simulation would strengthen the level of confidence and reliability of the model. Additionally, the studies did not include uncertainty analyses of the groundwater condition, which is particularly important in this region since the rate and spatial distribution of groundwater pumping is largely uncertain (Taufiq et al., 2018).

In this study, an integrated hydro-geomechanical model of the aquifer system underlying Bandung is developed to simulate the spatio-temporal relationship between subsidence and hydrogeology. A highly parameterized inverse modelling technique (White, 2018) is applied to reconstruct past groundwater extraction rates based on history-matching of InSAR observations and a small number of hydraulic head measurements. The resulting calibrated model allows us to understand the evolution of the groundwater exploitation in the urban area and quantify the long-term aquifer storage depletion. Future scenarios of aquifer exploitation until 2050 are also investigated to assess the long-term sustainability of different abstraction schemes and to simulate corresponding induced subsidence.

This study proposes a novel methodology for assessing land subsidence in data-sparse regions by integrating InSAR data with a hydro-geomechanical model. By leveraging InSAR's ability to measure ground deformation with high spatial and temporal resolution, our approach aims to bridge the data gap often encountered in groundwater studies since traditional data sources are often insufficient for detailed aquifer characterization and understanding of groundwater dynamics. By incorporating InSAR data as a calibration target within the hydro-geomechanical model, we seek to enhance the model's parameterization and improve our understanding of groundwater dynamics and associated land subsidence. This innovative approach offers a valuable tool for characterizing compacting aquifers and quantifying historical groundwater extraction, which is often unknown in many parts of the world.

2. Materials and methods

2.1. Study area

2.1.1. Geological and geomorphological setting

The focus of this study is the Bandung Basin in West Java, Indonesia (Fig. 1). The hydrogeological boundary is defined by the West Java Province's Office of Energy and Mineral Resources (ESDM) based on hydrogeological, geological, and groundwater hydraulic information. The city of Bandung lies within the predominantly flat basin centre and is surrounded by mountains reaching elevations up to 2500 m above sea level. The Citarum River passes through the basin and flows westwards towards the Saguling Reservoir. With annual precipitation of 1500 to 2500 mm (Taufiq et al., 2018), and potential evapotranspiration of 1560 mm (Siswanto and Francés, 2019), the climate in this region is described as tropical monsoon and is characterised by a rainy season (October to May) and a dry season (June to September) (Tirtomihardjo, 2016). The population within the basin surpassed 9.6 million in 2017 (Rusli et al., 2021)

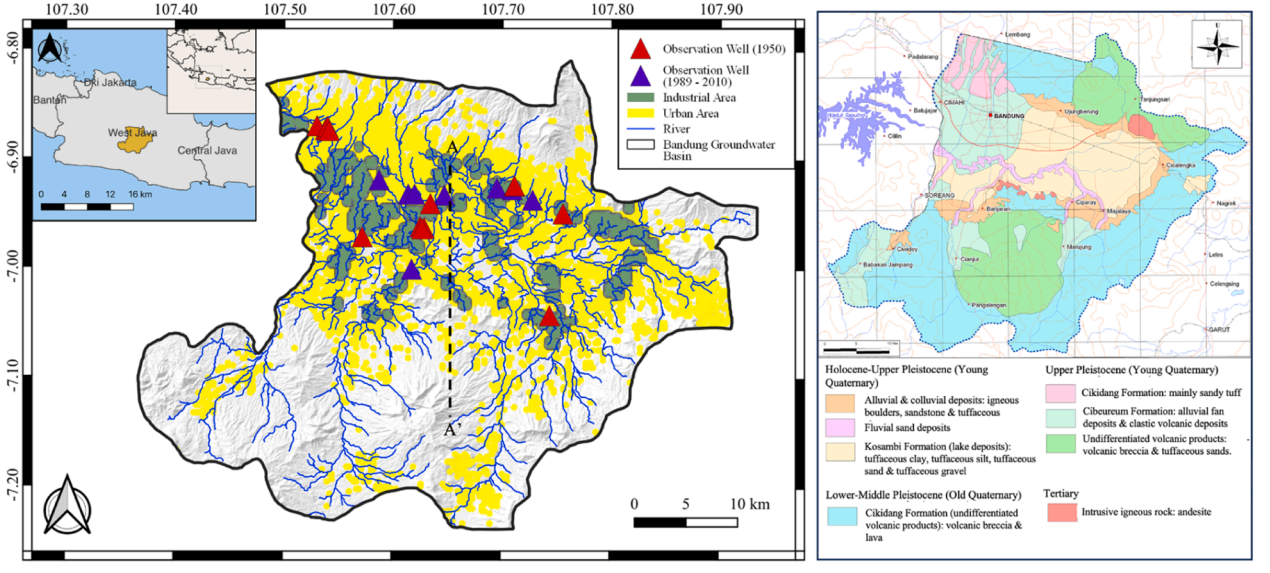

Fig. 1. Map of the Bandung groundwater basin (left). Locations of the groundwater level observations, and residential and industrial land cover are shown. Map of the geological units (right) obtained from the Indonesian Ministry of Public Works and Housing (PUPR; https://www.pu.go.id/).

and continues to grow at an annual rate of 1.2 % (Tirtomihardjo, 2016, p. 10). Bandung city is the major hub for economic and industrial activity within the province. The rise in population, urban expansion, growing tourism, and industrial development are primary factors intensifying the strain on the basin's groundwater system.

The study area consists of an alluvial plain surrounded by a mountainous chain of Quaternary volcanic rocks (Fig. 1). During the Lower Pleistocene, ongoing volcanic activity and uplift led to the deposition of the Cikapundung Formation, a 350 m thick layer comprising volcanic conglomerates, compacted breccias, tuffs, and andesitic interlayers. The deposits of this formation are highly compacted and form the basement of the aquifer system (Taufiq et al., 2018). During the Late Pleistocene to Holocene era, volcanic products filled the Bandung depression, forming the partially consolidated Cibeureum Formation, characterised by tuffs, breccias, and some lava intrusions up to 180 m thick. The Cibeureum Formation is interfingered with the Holocene age Kosambi Formation which is centrally located within the basin as a lake deposit consisting of unconsolidated claystone, siltstone, and sandstone (Hutasoit, 2009).

2.1.2. *Hydrogeological setting and aquifer exploitation*

In the Bandung groundwater basin, the Cibeureum Formation is the main aquifer, extending from the north to the south of the study area. The Kosambi Formation encompasses less permeable layers of tuffaceous clay and silt that are distributed throughout most of the basin acting as an aquitard within the primary aquifer. Regions near the mountains lack a consistent spatial distribution of these low permeability layers and thus the main aquifer remains undisturbed and functions as a continuous, deep aquifer in these locations.

The aquifer system can be divided into three layers (Rusli et al., 2023a, b): the shallow and deep aquifers composed of repeated sequences of breccia and tuff that are interspersed by a clayey aquitard, all of which overlay the volcanic bedrock. Fig. 2 illustrates the conceptual groundwater flow model along a north-south cross-section. The uppermost aquifer unit is considered unconfined with shallow groundwater accessible by dug wells generally at a depth of less than 25 m for domestic use (Agustin et al., 2023). The semi-confined to confined deeper aquifer is accessed by deeper drilled wells reaching up to 250 m according to available borehole logs (Rahiem, 2020), to supply water for industrial, commercial, and municipal purposes.

Groundwater meets 60 % of the total water demand in the Bandung groundwater basin (Taufiq, 2010). Groundwater extraction from the deep aquifer in the Bandung groundwater basin has been documented since the early 1900s and shown to steadily increase thereafter (Abidin et al., 2009). Groundwater extractions for domestic use are not regulated, and the shallow aquifer groundwater levels are not monitored (Rusli et al., 2021). Excessive groundwater withdrawals have altered the natural groundwater flow dynamics in the Bandung groundwater basin and created groundwater depression cones in some areas where industrial complexes are located (Taufiq et al., 2018). These industrial areas are dominated by textile factories, which have expanded in the region since the 1970s (Abidin et al., 2009). While there is strict legislation regarding the industrial use of groundwater from deeper aquifers in Bandung, the enforcement of water-related regulations in Indonesia has been challenging (Rusli et al., 2021). Therefore, the reported total annual groundwater extraction volumes are suspected to be underestimated. Taufiq et al. (2018) estimated that the actual groundwater extraction by industries was up to 14 times higher than reported volumes.

2.1.3. *Subsidence*

The monitoring of land subsidence in the Bandung groundwater basin started in 2000 using GPS methods (Abidin et al., 2013) with subsequent studies using InSAR techniques to study the phenomenon in the basin (Sri Sumantyo et al., 2012; Khakim et al., 2014; Du et al., 2018). Abidin et al., (2008)) and Ge et al. (2014) reported numerous subsidence zones in textile industry areas, where deep aquifer groundwater extraction occurs. Ge et al. (2014) compared InSAR-derived measurements with groundwater level measurements, confirming that a 20 mm decrease in ground surface corresponded to a 1 m decline in the groundwater table. Khakim et al. (2014) found that significant subsidence was associated with low permeability, compressible alluvial and lake deposit sediments. Gumilar et al. (2021) used InSAR results from 2016 to 2019 and found that high subsidence rates of up to 15 cm/yr within the centre of the basin corresponded with various evidence of subsidence-related damage such as cracks in houses, sunken and sloping houses, damage to roads, and expansion of the flood inundation area. Overall, prior research has linked land subsidence in the Bandung

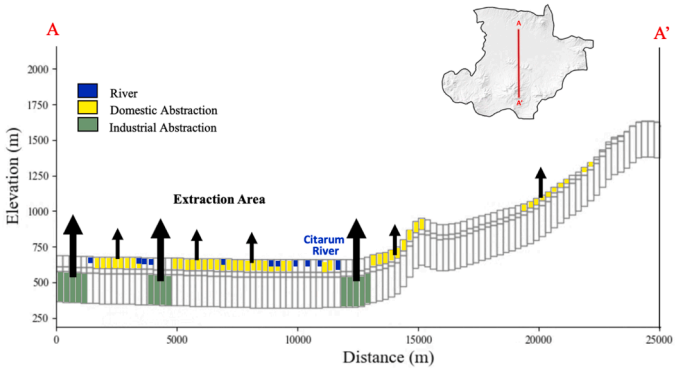

Fig. 2. Conceptual cross-section of the Bandung groundwater basin along the A'-A transect. The groundwater is mainly abstracted in the middle part of the basin from both the shallower unconfined aquifers by the domestic s e c t o r, and the deeper confined aquifers for industrial purposes.

groundwater basin to extensive groundwater extraction closely associated with the locations of textile and manufacturing industries which inherently rely on water for their operations. However, the mechanism of land subsidence in the Bandung groundwater basin is potentially complicated by additional factors such as the addition of building loads, natural consolidation of young sediments, and tectonics, as seen for example in Hanoi (Bateson et al., 2023).

A recent InSAR time series analysis from January 2015 to December 2020 within the Bandung groundwater basin showed widespread subsidence in the central basin with some areas subsiding at rates up to 18.7 cm/year (Rygus et al., 2023). (Rygus et al., 2023) identified 12 main subsidence patterns across the basin (Fig. 3) with three areas exhibiting accelerating subsidence over an area of 8 km^2, four clusters covering an area of 20 km^2 showing a linear subsidence trend, and five clusters showing a deceleration (7 km^2) in subsidence. The subsidence is concentrated in the central basin, characterised by the widespread and thick Late Quaternary alluvium and fluvial sediments. The sinking of the ground surface has resulted in detrimental effects on infrastructure, such as buildings, roads, and pipelines, as well as increased vulnerability to flooding (Gumilar et al., 2021).

In general, previous studies and the most recent InSAR data from 2015 to 2020 (Fig. 3) show that the Bandung groundwater basin is undergoing long-term subsidence trends with no apparent seasonal variations, likely due to groundwater extraction occurring primarily from the deeper, confined aquifer, which is less influenced by seasonal recharge (Chaussard et al., 2013). With no short-term variations of deformation observed compared to the long-term subsidence rates and with several studies showing groundwater decline across the basin with no significant rebound, we expect the subsidence to be the result of inelastic compaction of the aquifer system.

2.2. InSAR data

In this study we consider two InSAR datasets with displacement measurements over the Bandung groundwater basin. One dataset consists of ALOS PALSAR radar images acquired from July 2007 to February 2011 that had been processed by Prasetyo et al. (2013) using the PSInSAR (Permanent Scatterer Interferometry Synthetic Aperture Radar (Ferretti et al., 2001)) algorithm. The second dataset consists of Sentinel-1 radar images acquired from January 2015 to December 2020 that had been processed with the SBAS (Small BAseline Subset, (Berardino et al., 2002)) technique by Rygus et al. (2023). Further details of the two datasets can be found in Table 1.

We projected from satellite line-of-sight (LOS) measurements from the ALOS PALSAR and Sentinel-1 deformation time series to the vertical direction following the procedure described in Rygus et al. (2023). Time series measurements of the vertical component of motion provide history-matching targets for the numerical model. In accordance with our previous study in the Bandung basin (Rygus et al., 2023), we omitted the horizontal component of motion as the vertical component is the dominant direction of motion and directly related to subsidence.

Based on the results of our prior InSAR time series analysis in the Bandung groundwater basin (Rygus et al., 2023), measurement points (MPs) that displayed suspected non-groundwater ground surface movement observations (i.e., compaction induced by building loads) were removed from the current analysis in an attempt to focus on subsidence zones that are suspected to be mainly associated with groundwater level decline. To aid computational efficiency, we sampled 2500 random locations from the remaining MP dataset to use as model history-matching targets. (Fig. 4).

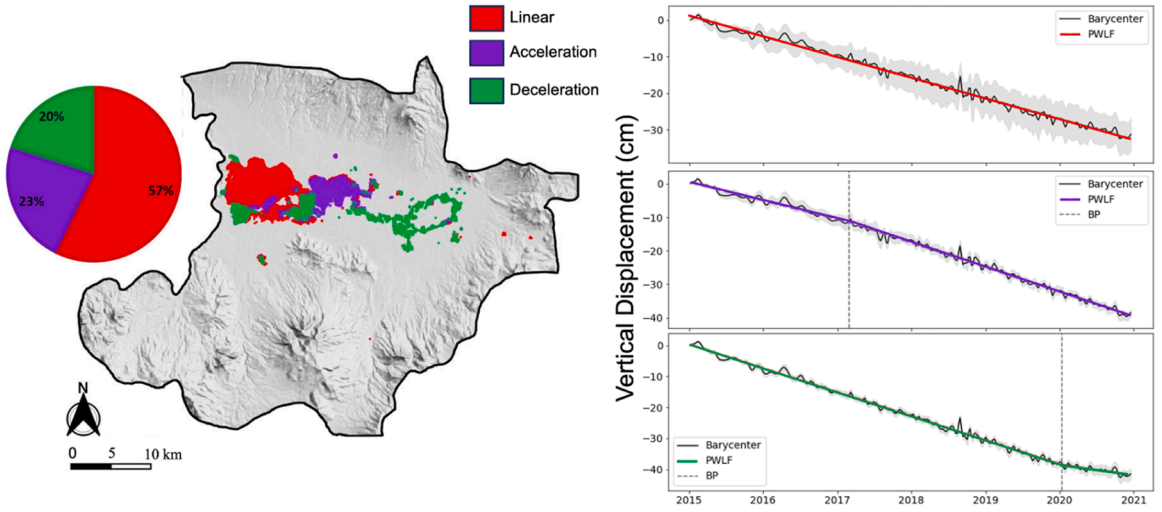

Fig. 3. The spatial distribution and percentage of InSAR measurement points (MPs) belonging to each of the subsidence trends identified in Rygus et al. (2023): linear, acceleration, deceleration (left); and representative displacement time series for each subsidence trend (right). The black line represents the cluster barycenter, the shaded grey area represents the 10 % and 90 % quantiles of MP time series within the cluster, the coloured lines reflect the linear segments of the fitted piecewise model, and the vertical dashed grey line indicates where a breakpoint was identified in the time series.

Table 1
Details of the InSAR datasets.

SAR data	Spatial resolution (m)	Radar sensor	Number of Images	Processing technique	Time span
ALOS PALSAR	30 × 30	L-band	19	PSInSAR	July 2007 to February 2011
Sentinel−1	5 × 20	C-band	344	SBAS	October 2015 to December 2020

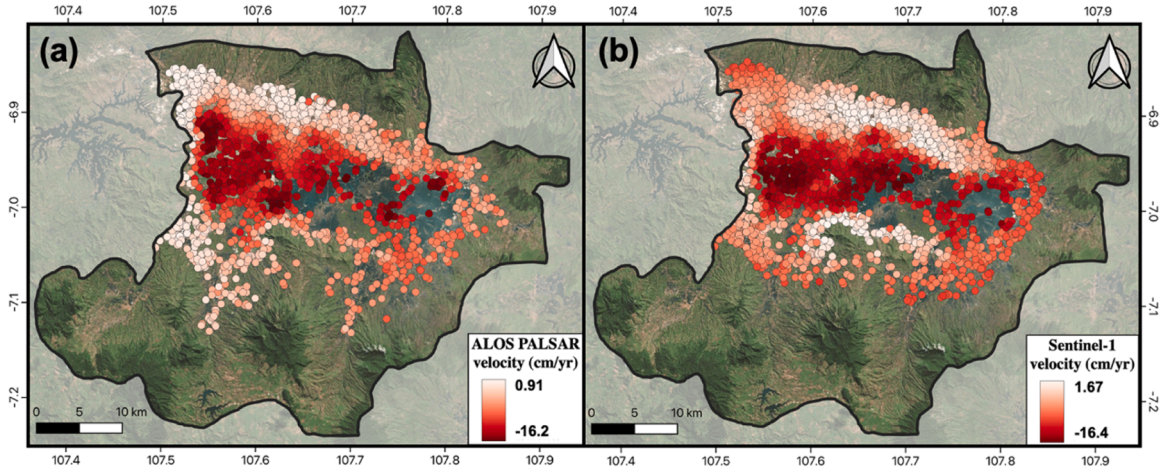

Fig. 4. Selected vertical velocity (displacement rate) observation points (a) derived from Prasetyo et al. (2013) using ALOS PALSAR PSInSAR data from 2007 to 2010; (b) Rygus et al. (2023) data derived from Sentinel-1 SBAS processing from 2015 to 2020.

2.3. Groundwater extraction-induced subsidence

Land subsidence resulting from groundwater extraction is a phenomenon observed in many aquifer systems that are at least partially composed of unconsolidated fine-grained sediments and have undergone substantial groundwater exploitation (Poland, 1984). The relationship between pore-fluid pressure changes and aquifer system compression can be explained by the principle of effective stress (Terzaghi, 1926). If the total stress on an aquifer system remains constant, the change in stress between sediment grains (effective stress) correlates with the change in pore-fluid pressure (Sneed, 2001) with the governing equation simplified and expressed in terms of the change of effective stress ($\Delta\sigma_e$), which is related to groundwater head (h) as:

$$\Delta\sigma_e = -\Delta u = -\rho g \Delta h \quad (1)$$

where σ_e is the change in effective stress, and Δu is the change in pore-fluid pressure, ρ represents the density of the water, g denotes the gravitational constant, and Δh is the change in hydraulic head.

MODFLOW 6 (Langevin et al., 2017) simulates groundwater flow and one-dimensional compaction using the CSUB package (Hughes et al., 2022) by combining Darcy's Law with mass balance and compaction through solving the equation:

$$\frac{d}{dx}\left(k_{xx}\frac{dh}{dx}\right)+\frac{d}{dy}\left(k_{yy}\frac{dh}{dy}\right)+\frac{d}{dz}\left(k_{zz}\frac{dh}{dz}\right)-(W+\underline{q}) = (1-\gamma) S_s\frac{dh}{dx} \quad (2)$$

where x, y, and z express the Cartesian coordinates; k_{xx}, k_{yy}, and k_{zz} designate the tensor components of hydraulic conductivity in the x, y, and z directions; h signifies hydraulic head; W represents the volumetric flux of water sources/sinks per unit volume; γ is the ratio of compressible interbeds volume over the total aquifer system volume; S_s is the specific storage which can be written as the sum of the specific storage due to the compressibility of water (S_{sw}) and the skeletal storage (S_{sk}); $\underline{q} = \gamma S_{sk}(\frac{dh}{dt})$ is the flow per unit volume for the compressible interbeds.

Specific skeletal storage values are contingent upon the head history of the compacting sediment. In instances where the head falls below the lowest preceding head (preconsolidation head), fine-grained materials undergo inelastic compaction involving a permanent rearrangement of the matrix skeletal structure and the collapse of pore spaces, which is characterised by a notably higher S_{sk} value. This collapse leads to irreversible compaction with the resulting water acting as a nonrenewable resource, accessible only at the cost of inducing land subsidence and diminishing aquifer system storage capacity. Inelastic compaction is typically negligible in coarse-grained sediments (Meade, 1964). Conversely, when the head remains above the preconsolidation head, deformation in both coarse- and fine-grained materials is elastic, with a considerably lower S_{sk} value. Elastic compaction refers to compaction where the skeletal structure of the sediments is not permanently altered and can be reversed by a corresponding increase in hydraulic head. For the same magnitude of changes in effective stress, inelastic compaction of fine-grained sediments can be one to two orders of magnitude larger than elastic compaction (Riley 1969b).

To account for the significant shift in S_{sk} when the effective stress surpasses the preconsolidation stress, it is common to utilise two distinct values:

$$S_{sk} = \begin{cases} S_{ske} \text{for} \sigma_e < \sigma_{e(\max)} \\ S_{skv} \text{for} \sigma_e > \sigma_{e(\max)} \end{cases} \quad (3)$$

Where S_{ske} and S_{skv} are the elastic and inelastic skeletal specific storages, respectively, and $\sigma_{e(max)}$ is the preconsolidation stress. For many fine-grained sediments, S_{skv} is one to three orders of magnitude greater than S_{ske} (Sneed, 2001).

For convertible model cells (i.e., cells which can be either confined or unconfined depending on the elevation of the computed water table), MODFLOW 6 uses a combination of specific storage and specific yield values to calculate storage changes. Under confined conditions, only specific storage is used whereas under unconfined conditions, both specific storage and specific yield are used. The CSUB package computes the storage changes is response to the groundwater level and the corresponding compactions for every model cell based on Eq. (2) and (3), using distinct storage terms based on whether the material is specified as non-compressible aquifer material or compressible interbeds (Hughes et al., 2022).

2.4. Numerical model

2.4.1. Spatial and temporal discretization

We developed a three-dimensional finite difference model using MODFLOW 6 (Langevin et al., 2017) coupled with the Skeletal Storage, Compaction, and Subsidence (CSUB) package (Hughes et al., 2022) to simulate aquifer-system compaction with groundwater flow. The CSUB package can simulate systems of fine-grained interbeds as a fraction of an aquifer system and computes the vertical (one-dimensional) compaction for the combined interbeds present within the specified aquifer.

The model domain covers an area of 1696 km^2 (Fig. 5) using a regular grid with 250 m x 250 m cells. Following the hydrogeological setting (see Section 2.2) the model is composed of three main layers: the top and bottom layers correspond to the unconfined and confined aquifer units of the Cibeureum Formation, while the middle layer represents the confining layer belonging to the Kosambi Formation. All cells within layer 1 in the model were simulated as convertible meaning that confined storage is used when groundwater head is above the cell top and a mixed formulation of unconfined and confined storage is used when head is below the top of the cell. The remaining layers were simulated as confined. The thickness of layers one and two were determined from the lithological profiles of 56 available borehole logs (Rahiem, 2020); while the bottom layer was assigned a uniform thickness of 250 m, ensuring that all monitoring wells were incorporated within the model.

The simulation period spans from 1950 to 2020 covering the groundwater level data availability and the period of exploitation of the aquifer that has led to the overall compaction of the aquifer system. The groundwater levels preceding 1950 were assumed to represent the natural condition of the aquifer system (i.e., before any major pumping commenced). Multi-year stress periods of 10

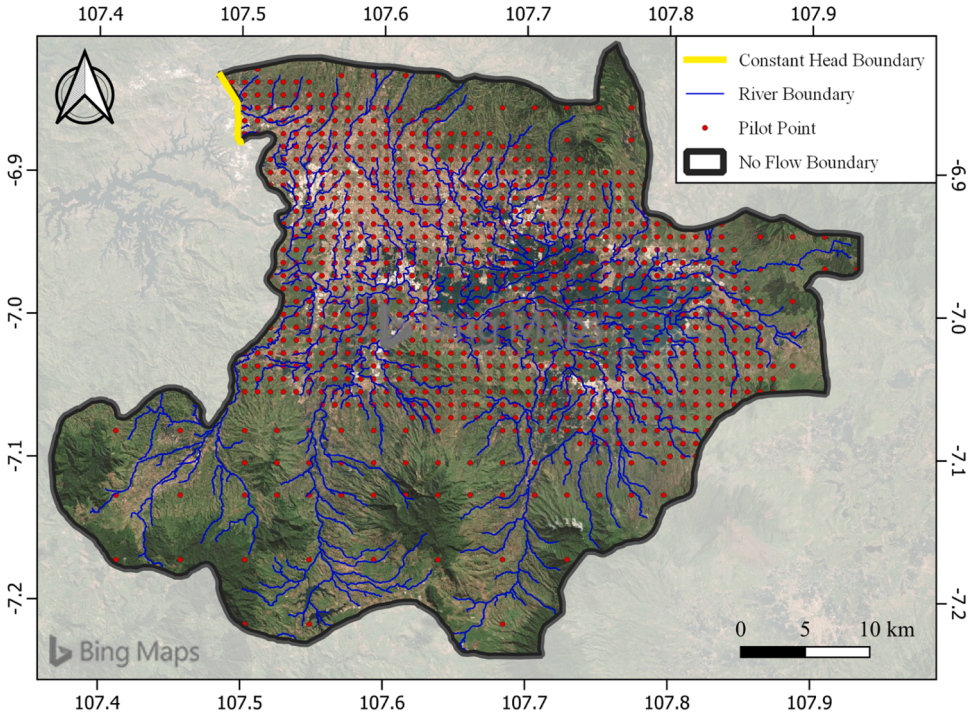

Fig. 5. Boundary conditions and pilot points used for parameterization of the Bandung Basin numerical model.

years were used from 1950 until 2000, thereafter annual stress periods were implemented, with the first stress period set as steady-state to provide the initial conditions for the subsequent transient stress periods.

2.4.2. Model parameterization

The main water input for the Bandung groundwater basin aquifer system is recharge from precipitation, which was simulated using MODFLOW's RCH package (Langevin et al., 2017). Annual precipitation data was obtained from standard data sources (Deutscher Wetterdienst 2022, Funk et al., 2015). This precipitation data is integrated into the model as spatially varied rainfall-to-recharge ratios based on the occurrence of built-up or vegetated land cover (a parameter optimised through history-matching) to derive net recharge. The net recharge rates are imposed over all cells at the top of the model and represent effective rainfall, as evapotranspiration processes are not explicitly simulated by the model.

No-flow boundary conditions are placed along the hydrogeological basin boundary (Fig. 5) except for the north-western boundary of the aquifer system which is defined as a constant head boundary condition to represent an exchange of lateral flow where a physical boundary to flow is absent. The initial head values used to parameterize this boundary are derived from the temporal evolution of the nearest existing observation wells.

The initial values for the hydraulic and aquifer properties, including the horizontal and vertical, hydraulic conductivities of each layer and the specific yield, are derived from available in-situ slug tests, laboratory results, and pumping test reports, as described in (Rusli et al., 2023a).

Under natural conditions, the groundwater is discharged to the Citarum River. The river and its major tributaries are simulated in the model using MODFLOW's RIV package (Langevin et al., 2017). The initial riverbed conductance was set to 50 m^2/d based on the vertical hydraulic conductivity of the top aquifer unit. In view of the limited information available on conductance values and for simplicity, homogeneous values were used for each river and estimated during the model inversion process discussed in Section 3.4.

Groundwater pumping is known to occur within the basin; however, the spatial distribution of the wells and the actual pumping rates are not known. To simulate the domestic use of groundwater, wells are included in the unconfined aquifer (layer 1) with withdrawal volumes estimated from the annual extraction rates reported by (Rusli et al., 2021) from 2005 to 2018, which we further extrapolated using an exponential model to cover the time period of the simulation. The industrial groundwater extractions are simulated with wells withdrawing water from the deeper confined aquifer (layer 3) with the initial rates derived from previously simulated groundwater pumping volumes (Taufiq et al., 2018; Rusli et al., 2023b).

To determine the spatial distribution of groundwater extraction for the unconfined and confined aquifer units, annual true colour images were compiled using Landsat-3,-4,-5,-7 and Sentinel-2 satellite imagery obtained via the Google Earth Engine platform starting from 1978 (when Landsat-3 data was first available) until the end of 2020. The resulting images were subjected to colour filtering using OpenCV (Bradski, 2000), a computer vision Python package, exploiting the noticeable colour differences in the images between the industrial areas, the residential areas, and the vegetated areas in order to extract the spatial locations of residential and industrial land cover. The annual domestic and industrial groundwater extraction rates were uniformly distributed throughout the respective areas in the model by inserting a model well within each cell within a residential or industrial area (Fig. 1).

The head-based formulation of the CSUB package was used to simulate compaction of aquifer materials. Fine-grained materials were initially assigned uniform vertical hydraulic conductivity and porosity values derived from one-dimensional consolidation tests that were performed on core samples collected from three field sites located in the eastern portion of Bandung. The inelastic skeletal specific storage of the sample can be estimated by computing the ratio of the vertical hydraulic conductivity to the coefficient of consolidation (Jorgensen, 1980) as follows:

$$S_{skv} = \frac{K_v}{c_v} \tag{4}$$

Where both c_v, the coefficient of consolidation, and K_v, the vertical hydraulic, are calculated from the consolidation test results.

For the remaining storage parameters, we used a priori parameter ranges obtained from previous studies as starting values for the model history-matching process (Calderhead et al., 2011; Li et al., 2022; Chowdhury et al., 2022).

CSUB parameters of representative interbed thickness ("thick_frac") and the representative number of interbeds ("rnb") were estimated for each model layer based on observed ratios of sand and fine-grained sediment at 56 borehole locations (Rahiem, 2020). These property values were subsequently spatially interpolated from the borehole locations to all active model cells. Following the procedure outlined in Ellis et al. (2023), an auxiliary parameter named "clay_frac" was introduced in order to simulate variable proportions of fine-grained sediment (interbeds or confining units) to coarse-grained sediment in each cell during the history matching of the model. The initial value of "clay_frac" for every model cell was determined by multiplying the "thick_frac" by the "rnb" and then dividing the result by the total cell thickness. The parameterized "clay_frac" value was used to retroactively calculate an optimised value of "thick_frac". This indirect parameterization method was essential for preventing combinations of CSUB input values that could unrealistically result in the total interbed thickness exceeding the cell thickness.

The specified initial preconsolidation head in the CSUB package governs the initiation of inelastic compaction. The pre-consolidation head is continually updated to the effective stress at the end of each annual time step when the preconsolidation stress is exceeded. This initial head is defined as drawdown below the groundwater level in the first stress period (steady state), and subsequent elastic or inelastic storage coefficients are applied based on the relationship between the modelled groundwater level and the current preconsolidation head. Roughly, the initial preconsolidation head can be derived from the groundwater level at which the rate of subsidence first markedly increased (Holzer and Pampeyan, 1981; Galloway and Burbey, 2011). Due to the lack of subsidence data in

the Bandung groundwater basin prior to 2000, the initial preconsolidation head is set to be the same as the predevelopment initial heads from 1950 that are assumed to represent natural condition before the onset of heavy pumping. Head offsets were set to an average value of 0.5 m, 1.0 m, and 1.6 m for model layers 1, 2 and 3, respectively.

Pilot point parameterization (Doherty, 2003) was used for all parameter groups (Fig. 5), apart from the river, well, and constant head boundary conditions for which we used grid cell parameterization. Pilot points were placed more densely at a separation distance of 500 m in the basin centre which is heavily impacted by subsidence (Fig. 4) and more sparsely elsewhere in the model domain resulting in a total of 997 pilot points in each layer for the corresponding parameter groups. Exponential variograms were used to capture the spatial covariance between pilot point and grid-scale parameter values. Multiplier parameters are used whereby the initial input values are multiplied by a value selected within a parameter range to represent uncertainty. Upper and lower limits are placed on each multiplied parameter value to ensure that the resulting value remains within a realistic range of values. A summary of the parameter limit range and the prior estimates of the hydraulic conductivity and storage parameters are shown in Supplementary Table S1 of the Supplementary Material, with the mean of the prior probability distribution representing the preferred value during the history matching process.

2.5. Model history matching

Model history-matching involves adjusting the initial parameter values of a model to enhance the agreement between the simulated data and historical observations. This process involves modifying parameter values to minimise the discrepancy, or residual, between observed historical data and their simulated counterparts within an ensemble. In a Bayesian framework, history matching combines information from two sources: the aquifer-specific details from historical observations and the aquifer system knowledge embedded in the prior parameter distribution.

An ensemble-based history-matching algorithm was employed through the use of a tool called PESTPP-IES (White, 2018) with the Python framework for Environmental Modeling Uncertainty analyses (pyEMU) (White et al., 2016) interface. PESTPP-IES uses an ensemble-smoother iteration of the Gauss-Levenberg-Marquardt algorithm to approximate a Jacobian matrix by leveraging empirical correlations between parameters and simulated outcomes. It adapts the entire parameter ensemble simultaneously, providing a range of calibrated parameter fields for uncertainty evaluation without additional history-matching costs. This approach efficiently addresses nonlinear uncertainties, facilitates probabilistic predictions, and optimises computational efficiency, particularly in models with extensive parameterization.

In this work, the objective function incorporates historical observations of groundwater levels and InSAR-derived measurements of land displacement with observation weights specified during history matching to ensure that the contribution of each observation type aligns optimally with the model's intended decision-support objectives (Anderson et al., 2015).

The following observations comprise the history-matching dataset:

- Steady state groundwater heads measuring the groundwater condition in 1950 from 10 observation wells (Fig. 1);
- Transient head measurements from 1989 to 2010 in eight observation wells (Fig. 1);
- ALOS PALSAR InSAR ground displacement measurements of 2500 MPs from 2007 to 2011 (Fig. 4).
- Sentinel-1 InSAR ground displacement measurements of 2500 MPs from 2015 to 2020 (Fig. 4).

Due to the absence of InSAR data between the ALOS PALSAR and Sentinel-1 datasets (2012–2014), this period was excluded from the model history-matching process. Model history-matching was conducted using only the available historical data.

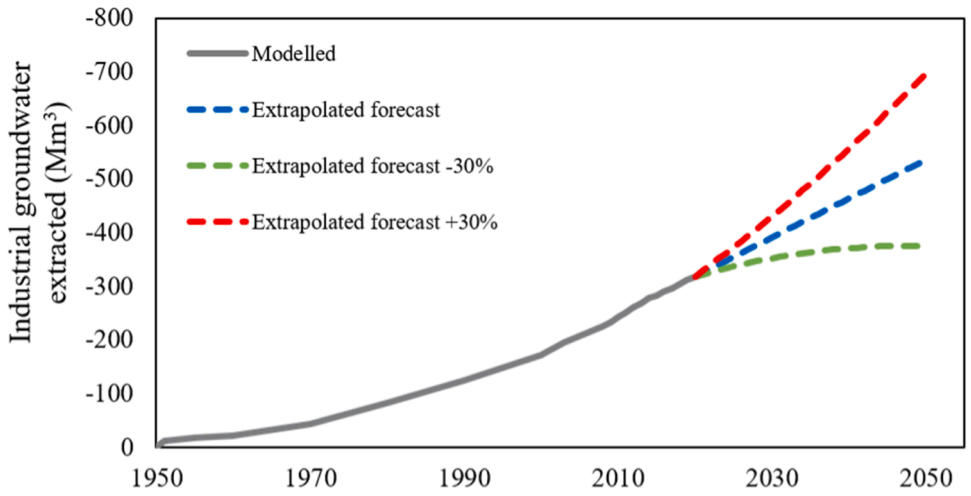

Fig. 6. Volume of groundwater extracted as represented by the mean ensemble forecasted until 2050 under varying pumping conditions.

The observation weighting scheme was designed to assign equal importance to both the matching of hydraulic heads and the ground displacement measurements during the history-matching procedure. PESTPP-IES generated observations with noise ensembles to investigate posterior parameter uncertainty, using observation weights to estimate measurement errors. Error bounds of ± 0.5 m were applied to groundwater levels from observation wells, and ± 20 % for the InSAR-derived displacement measurements.

2.6. Scenario forecasting

To investigate future aquifer storage loss and estimate additional land subsidence induced by groundwater exploitation in the Bandung groundwater basin, we included a forecast period from 2020 to 2050, which was discretized into 30 stress periods of 1 year each. The 30-year forecast period incorporated the average stresses observed during the final three years of the model's transient period (2017–2020), apart from the well pumping rates, which were varied to assess the impact of different pumping regimes (Fig. 6). Similar to the work by Ceccatelli et al. (2021), we considered three different pumping scenarios from 2021 to 2050:

1. "Business-as-usual": No deviation in the recent trend of industrial groundwater extraction. The recent modelled pumping rates (from 2017–2020) were linearly extrapolated to represent a continuation of the recent trend (blue line in Fig. 6).
2. Decreasing pumping rates: A decrease in industrial groundwater extraction by an average of 1 % per year from 2020 onwards, resulting in a cumulative decrease of 10 % by 2030, 20 % by 2040, and 30 % by 2050 (green line in Fig. 6). Decreasing the pumping rates is based on the assumption of improvements in industrial water management.

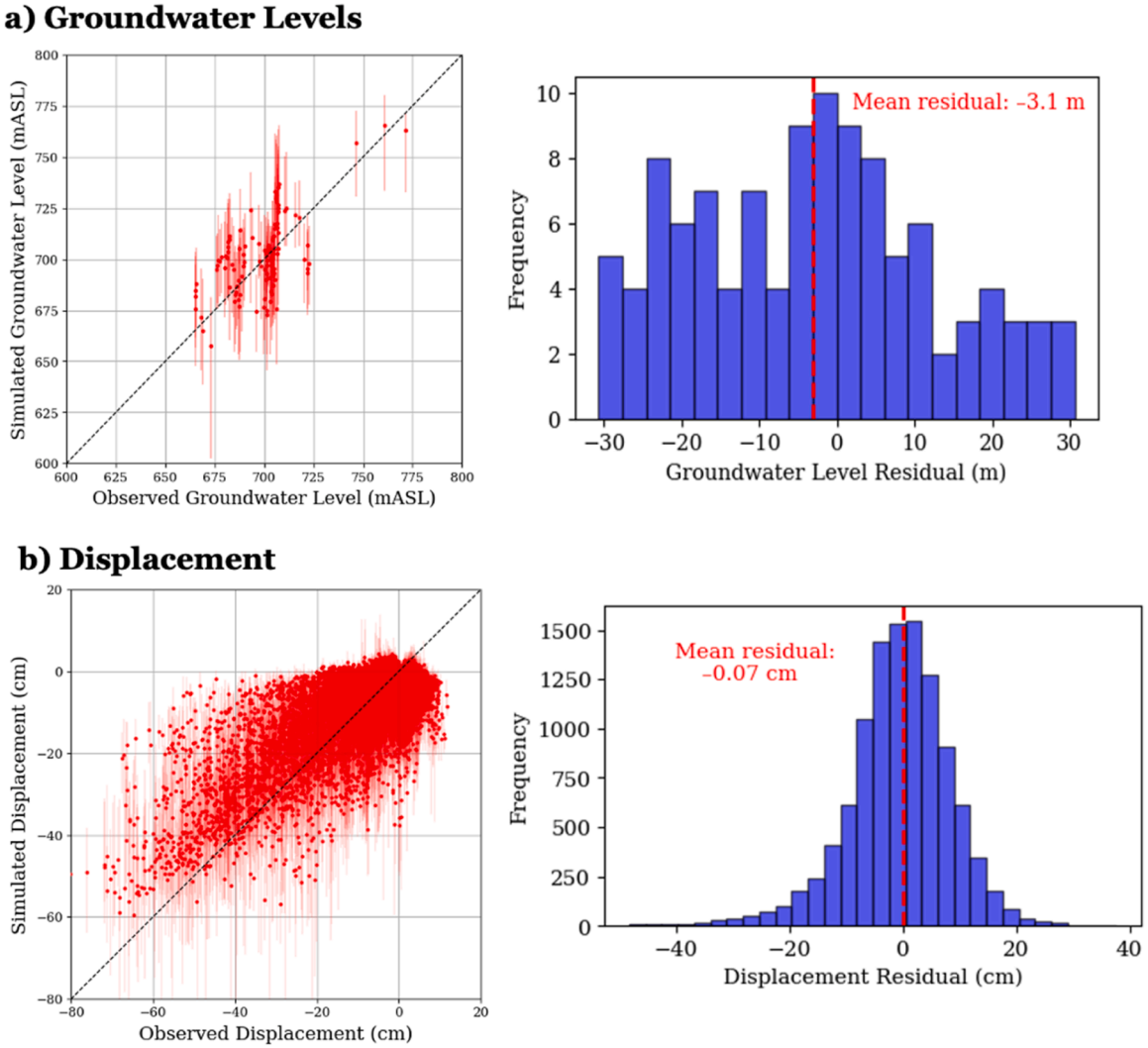

Fig. 7. Scatter plots with the points representing the ensemble mean and the bars representing the minimum and maximum ensemble values (left) and corresponding distribution of residuals (right) for simulated to observed data for the (a) groundwater levels and (b) ground displacement measurements.

3. Increasing pumping rates: An increase in the industrial groundwater extraction by an average of 1 % per year from 2020 onwards. This leads to a cumulative increase of 10 % by 2030, 20 % by 2040, and 30 % by 2050 (red line in Fig. 6). Increasing pumping rates assumes an increase in economic activity and associated pressures on natural resources, given that Indonesia is expected to become the fourth largest economy worldwide by 2050 (Organisation for Economic Co-operation and Development OECD, 2018).

The analysis assumes that current pumping rates and water dynamics remain constant throughout the projection period.

In all forecast scenarios, the domestic use was projected to increase by 1 % each year following recent population data (Rusli et al., 2021).

3. Results

3.1. Model history matching

A prior parameter ensemble comprising 150 realisations was enforced in accordance with (Hunt et al., 2021) who suggested that an ensemble size between 50 and 150 realisations is appropriate for most environmental modelling applications. The history matching process involved 663 forward model runs. The ensemble resulting from the final iteration was conditioned to eliminate model realisations with an objective function score equal to or exceeding the 95th percentile. This led to a conditioned posterior ensemble, consisting of 142 model realisations.

The evaluation of the history-matched ensemble fit to observations was conducted by assessing the reduction in residuals between historical observations and their simulated counterparts. The history-matching performance of the model ensemble for all observation groups is shown in Fig. 7.

For the groundwater levels, the scatter plot shows a satisfactory match between the observed and simulated values (Fig. 7a), with no discernible bias observed in the simulated heads as evident from the cloud of points being centred around the 1:1 line. The model residuals are on average equal to –3.1 m and result in a scaled root mean square error (SRMSE, calculated as RMSE divided by the observation range) of 14.2 %. This shows that the model shows a moderate overestimation of the groundwater levels. Since the locations of pumping wells are unknown and instead prescribed to the model as described in section 3.3.2, this uncertainty in the location of groundwater extraction may also lead to underestimation of pumping rates in some areas, and a higher simulated groundwater level compared to observed measurements.

For the displacement observations, we found a generally a good agreement between the observed and model-simulated groundwater levels with most simulated displacement values plotted on or near the 1:1 line (Fig. 7b), and. The model residuals are equal to –0.07 cm on average with a SRMSE of 11.3 %.

The posterior parameter ensemble yielded hydrogeologically plausible values (Supplementary Table S1 of the Supplementary Material) that were within the ranges of previously published values from (Rose, 1945; Taufiq et al., 2018; Rusli et al., 2023) and agree with the current understanding of the spatial and temporal patterns of parameter uncertainty for the Bandung groundwater basin aquifer system.

Maps of the simulated ground displacement coincide with the spatial distribution of the observed rates for the time periods covered by both the ALOS PALSAR and the Sentinel-1 data (2007–2010 and 2015–2020, respectively) (Fig. 8). In particular, the simulated rates show a good agreement with the high subsidence rates found throughout the western portion of the basin (Fig. 8). The highest

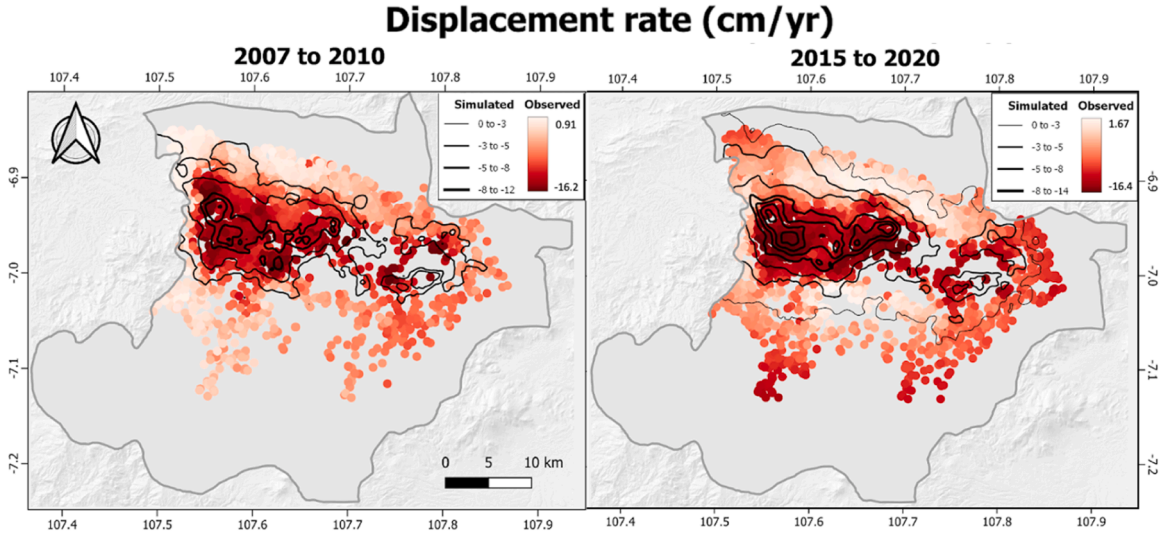

Fig. 8. Comparison of the simulated displacement rates with the (a) ALOS PALSAR observations from 2007 to 2010, and (b) Sentinel-1 observations from 2015–2020.

subsidence rates (16.2 cm/yr and 16.4 cm/yr for the ALOS and Sentinel timeframes, respectively) are located in the centre of the western subsidence bowl.

Fig. 9 shows the distribution of the cumulative subsidence simulated over the modelled time period (1950–2020) with the highest cumulative subsidence (up to 6.9 m) evident within the central and western portions of the basin where thicker layers of fine-grained sediments are present. Fig. 9 also displays a comparison of simulated and observed time series for select InSAR MPs located in the areas showing the highest cumulative subsidence. The simulated subsidence time-series produced by the posterior ensemble of model realisations generally brackets the historical subsidence observations and estimations at most of the MPs included in the model, indicating that the posterior ensemble can reproduce many aspects of the observed historical subsidence processes.

The simulations for the period 1950–2020 provide information about how the aquifer units contributed to overall compaction due to the continual lowering of groundwater levels. A total of 2.4 m (0.3–6.3 m, 5 % - 95 % range) of compaction was simulated for the period 1950–2020 averaged across the model extent. Of the total simulated compaction, the shallow aquifer unit accounted for 28–30 % while the deep aquifer unit accounted for 68–72 % (Table 2).

3.2. Groundwater usage across the Bandung groundwater basin

We have simulated widespread groundwater drawdown centres exhibiting a substantial decrease in water levels, with an overall drawdown of up to 25 m in the unconfined aquitard (layer 1) and up to 240 m in the deeper aquifer unit (layer 3) between 1950 and 2020 (Fig. 10). The impact of groundwater extraction on the groundwater heads is especially visible in the deeper aquifer as indicated by the closely spaced closed contour lines (Fig. 10). Specifically, areas with dense industrial complexes, for example in the western portion of the study area, demonstrate higher drawdowns within the deep aquifer unit compared to other urban areas. The drawdown contours in these areas coincide closely with the simulated subsidence (Fig. 10). The groundwater drawdown of the unconfined aquifer unit (layer 1) shows a similar spatial distribution, however not to the same extent as the deeper, confined aquifer (layer 3).

The temporal evolution of possible groundwater extraction volumes simulated in our model is shown in Fig. 11. The mean domestic groundwater use, representing groundwater extracted from the unconfined shallow aquifer, was simulated to increase up to a value of 119 Mm^3 (48–227 Mm^3, 5 % - 95 % range) by the end of the transient model simulation. The mean volume of industrial groundwater extraction from wells located within the confined aquifer continually increased by about 1 % in the last decade, eventually reaching an annual pumping volume of 381 Mm^3 (157–740 Mm^3, 5 % - 95 % range) in 2020. From 1950 to 1970, the simulated domestic and industrial groundwater use volumes were similar in magnitude and then diverged with the industrial usage dominating the extraction of groundwater for the remainder of the modelled period.

The spatial distribution for groundwater extraction rate from the mean posterior ensemble in 2020 is shown in Fig. 12. The highest rate of extraction in the deeper confined aquifer unit (13.6 Mm^3/yr) is in the central-western portion of the basin where several industrial complexes are located (Fig. 1). This portion of the basin is also associated with groundwater extracted from the shallow unconfined aquifer as the land between the industrial buildings is predominantly covered by residential buildings.

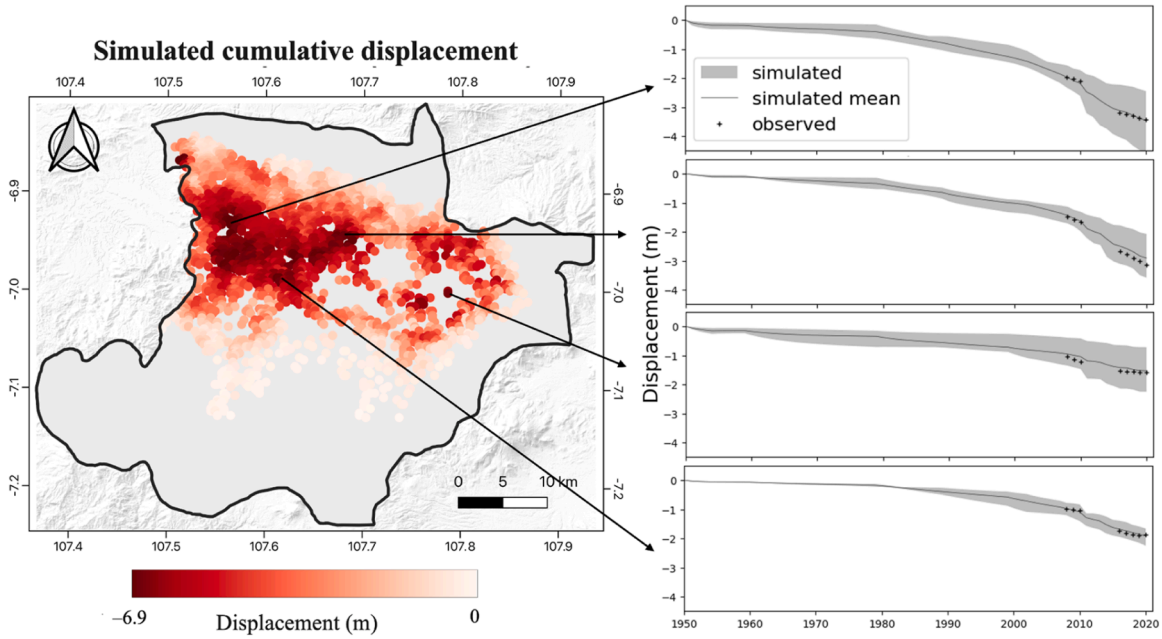

Fig. 9. The simulated cumulative subsidence over the modelling period (1950–2020) (left) and representative displacement time series at InSAR MPs with high subsidence (right). The shaded grey colour indicates the range of results simulated by the posterior ensemble of realisations, the black line represents the mean value of the ensemble and the black crosses indicate the values of observed displacement from InSAR measurements.

Table 2
Total simulated compaction from 1950 to 2020 averaged across model extent.

Model Unit	Simulated Compaction (m)			
	Mean	5th percentile	95th percentile	% of total compaction
Shallow aquifer	0.7	0.09	1.8	28–30
Deep aquifer	1.7	0.2	4.2	68–72
Total compaction	2.4	0.3	6.3	100

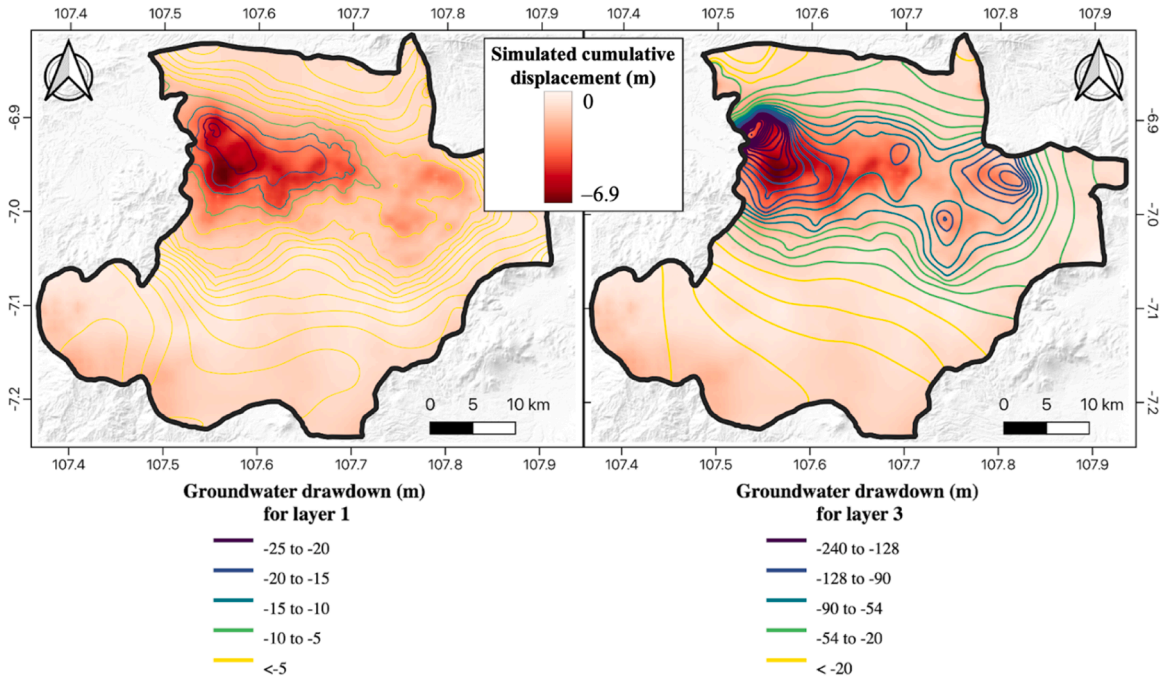

Fig. 10. Comparison of the simulated groundwater level drawdowns at the end of the transient model period (2020) relative to the steady-state condition (1950) in the upper, unconfined aquifer unit (left) and the deep, confined aquifer unit (right) with the total simulated cumulative ground displacement.

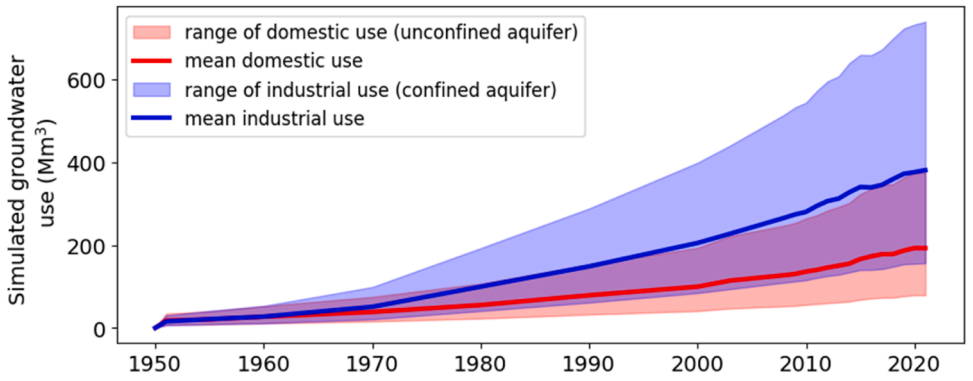

Fig. 11. Simulated temporal distribution of groundwater use over the model domain from 1950 to 2020 with the ensemble mean indicated by the solid line and the shaded regions indicate the 5th–95th percentile uncertainty from the ensemble.

Hydraulically, this area corresponds with a large depression cone in the deep confined aquifer, which is also observed in the shallow unconfined aquifer, albeit to a lesser degree (Fig. 10). In terms of land subsidence, we found the maximum cumulative simulated land subsidence (Fig. 9) collocated with the area that had the highest groundwater use from the confined aquifer.

Additionally, groundwater is also pumped in large volumes from the confined aquifer in the eastern region of the basin. These

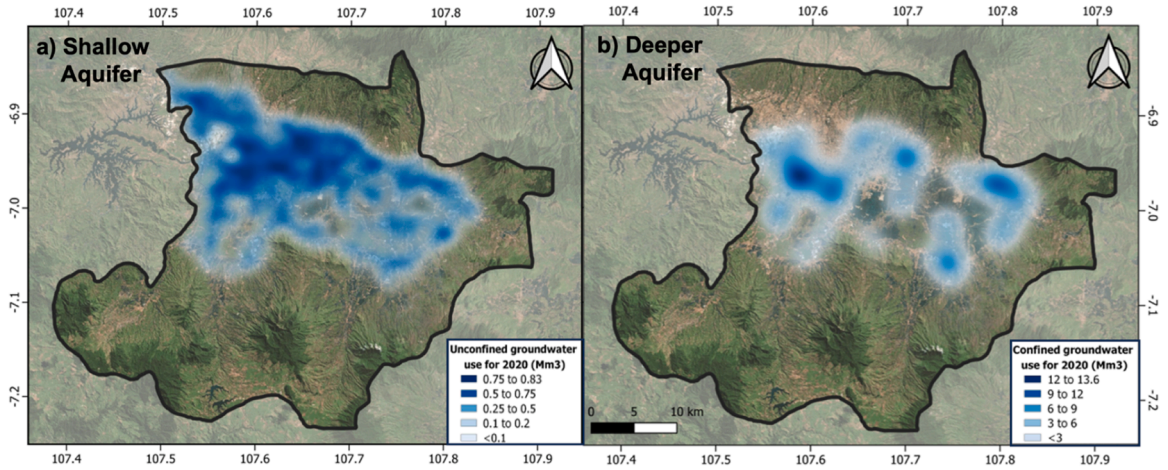

Fig. 12. Simulated spatial distribution of extracted groundwater over the model domain in 2020 for the a) shallow aquifer and the b) deeper aquifer.

eastern areas of high industrial pumping (up to 11.5 Mm^3/yr) correspond to total simulated subsidence of up to 3.2 m between 1950 and 2020.

3.3. Long-term aquifer storage capacity

The water budget for the Bandung groundwater basin's aquifer system for the mean posterior ensemble values includes mean annual inflows, outflows, and the net change in storage for the model period (Table 2). The sum of the simulated values of the outflows (1.8×10^6 m^3/yr) and the elastic expansion of the fine-grained sediment and numerical solver error (-67,300 m^3/yr) minus the inflows (1.5×10^6 m^3/yr) represents the reduction of storage from the aquifer system (268,700 m^3/yr).

Most of the in-elastic aquifer storage depletion in the Bandung groundwater basin is the result of the long-term groundwater-level declines described in Section 2.2. On average, the magnitude and duration of these groundwater-level declines resulted in largely permanent loss of aquifer storage as most of the water (on average 96 %) was derived from inelastic compaction of fine-grained units during the modelled period (Table 3). We see the reduction of storage steadily increase during the modelling period (Fig. 13), concurrent with the increased levels of pumping.

At the end of the model simulation period (2020), which is also the year of greatest simulated groundwater use (1.2×10^6 m^3; Fig. 13), the total volume of water released via inelastic compaction of the fine-grained units amounts to 7.0×10^3 m^3 in 2020. Thus, about 60 % of the total groundwater use in 2020 represents a permanent loss of water from the fine-grained sediments. The cumulative water released from storage over the model simulation period (1950–2020) was 7.4 km^3, of which 97 % of the water was derived from fine-grained units due to inelastic compaction (7.2 km^3; Fig. 13). This represents the total volume of the aquifer's storage capacity that has been permanently lost.

Table 3
Mean annual water budget for the posterior ensemble.

Water-budget category	Amount (m^3/yr)	Percentage of water budget
Inflow		
Recharge	1.0×10^6	96
Flow from adjacent aquifer (Constant Head package)	4.7×10^4	4
Total Inflow	1.5×10^6	100
Outflow		
Groundwater use (domestic)	3.2×10^5	18
Groundwater use (industrial)	6.4×10^5	35
River base flow (River package)	8.2×10^5	46
Flow to adjacent aquifer (Constant Head package)	1.7×10^4	1
Total Outflow	1.8×10^6	100
Net change in storage		
Water derived from specific yield under unconfined conditions	5.3×10^3	2
Water from fine-grained unit inelastic compaction	2.6×10^5	96
Water from coarse-grained unit elastic compaction	3.2×10^3	1
Contribution of water compressibility	1.2×10^3	1
Total storage change	2.7×10^5	100

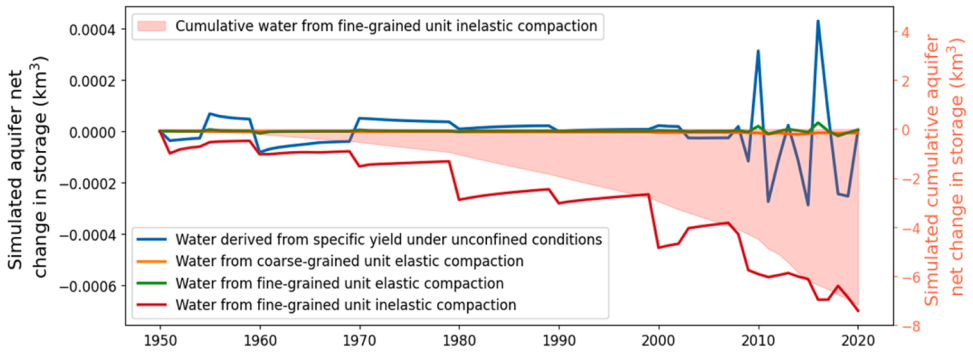

Fig. 13. Simulated water source and change in storage for the mean posterior ensemble over the transient model period (1950–2020).

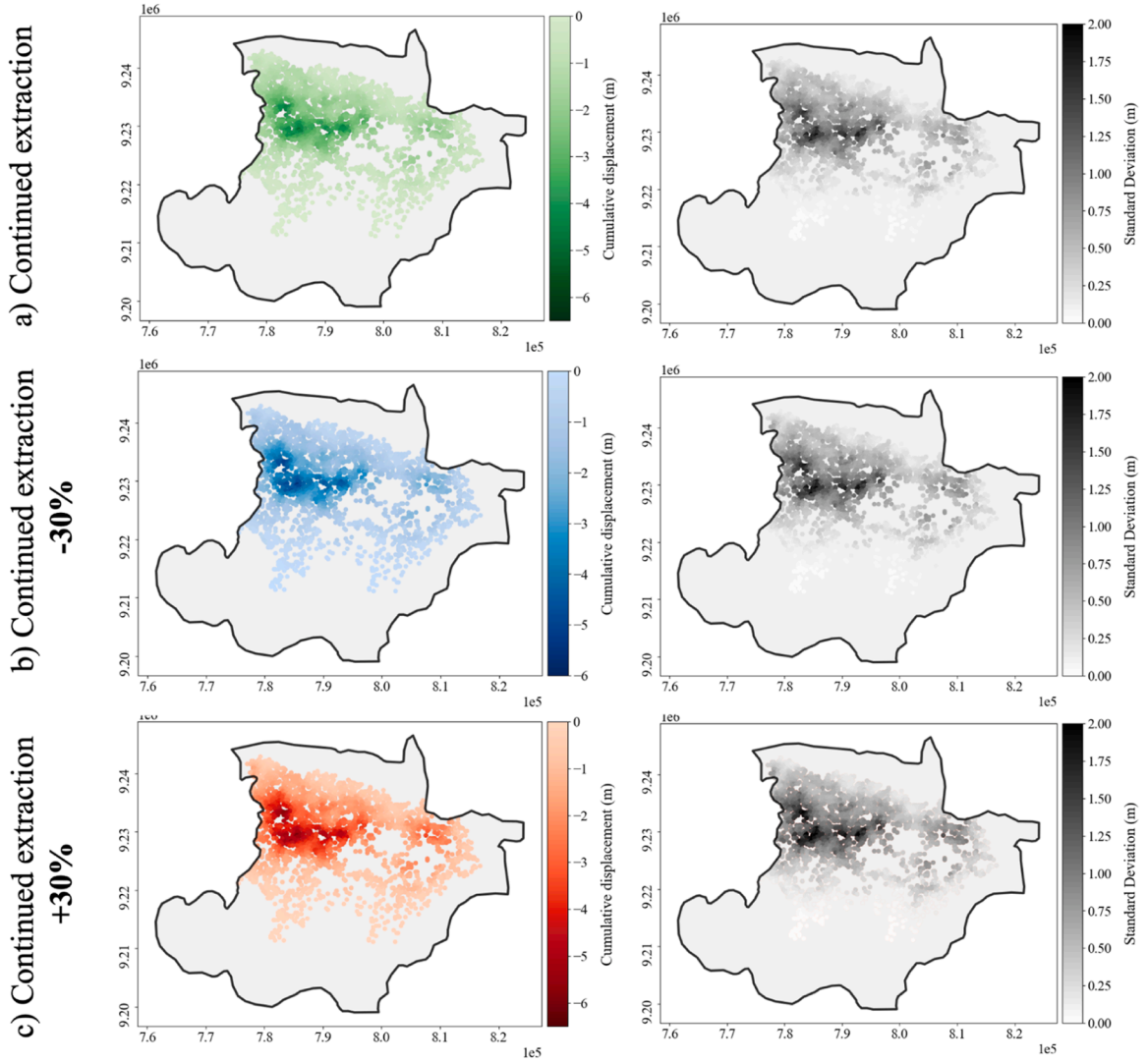

Fig. 14. Scenario results of subsidence (2020–2050) assuming: (a) continued extraction; (b) continued extraction rates −30 % by 2050; (c) continued extraction rates + 30 % by 2050. The mean values of the ensemble of realisations are given on the left, while the standard deviation of the ensemble values is shown on the right.

3.4. Subsidence forecasts for future pumping scenarios

We explore future subsidence due to continued groundwater pumping from 2020 to 2050 under three scenarios (Fig. 6). The first scenario assumes "business-as-usual" with no changes in the current (2020) industrial groundwater extraction rates. In the second scenario, we assume a reduction in groundwater extraction rate driven by stronger enforcement of industrial pumping regulations. The third scenario reflects increasing groundwater pumping, which is a proxy for continued unregulated urbanisation and increasing economic activity in Bandung city and therefore further pressures on groundwater resources. Notably, we assumed that the spatial distribution of the future pumping remains the same as that in 2020 (i.e., the expansion of groundwater pumping as a result of urban growth is not considered).

The results from our scenarios are shown in Fig. 14. For the simulated scenarios, the spatial distribution of the cumulative subsidence is consistent with the pattern observed at the end of the history-matched model simulation representing the 2020 condition. The important difference is the magnitude of subsidence. Extrapolating the recent modelled trend in groundwater extraction from 2021 to 2050 leads to additional subsidence up to 5.6 m ($\pm$ 1.1 m) within the widespread subsidence bowl located in the central-west portion of the basin. Subsidence within the eastern portion of the basin is less pronounced and reaches a maximum cumulative subsidence of 2.9 m ($\pm$ 1.2 m).

With a 30 % decrease in groundwater extraction by the end of 2050, we expect further subsidence of up to 5.1 m ($\pm$ 1.0 m) in the area of west Bandung, while in the eastern subsidence area we expect up to 1.9 m ($\pm$ 0.6 m) of subsidence (Fig. 14b).

With an increase in groundwater extraction of 30 % by the end of 2050, the model simulates further land subsidence reaching a maximum of 6.3 m ($\pm$ 1.2 m) in the western portion of the basin and up to 2.6 m ($\pm$ 0.9 m) in the eastern region (Fig. 14c).

Further permanent loss of aquifer storage capacity due to land subsidence occurs in all investigated scenarios. In the case of groundwater extraction linearly extrapolated based on the recent modelled trend (shown as the blue, dotted line in Fig. 6), an additional 11.1 km^3 of storage capacity would be lost by 2050, with 85 % of the water derived from fine-grained unit inelastic compaction. In the scenario where the groundwater extraction was reduced by 30 %, we expect an additional irreversible loss of 9.2 km^3 in aquifer storage capacity from 2020 to 2050. A forecasted increase in groundwater usage will result in a permanent loss of aquifer storage amounting to an additional 13.0 km^3.

4. Discussion

Conducting a hydrogeological assessment of the land subsidence in an area with limited data presents numerous challenges and uncertainties, especially when critical information on the temporal measurements of groundwater levels, are largely unavailable or unreliable. These data are particularly important for numerical models which are often used as tools for understanding subsurface phenomena that lead to surface ground deformation. Satellite-based InSAR techniques offer comprehensive spatial and temporal descriptions of ground surface displacements at basin-scale which can supplement groundwater levels as model calibration targets to improve numerical modelling and characterisation of aquifer systems undergoing compaction. In this study, we used this capability to enhance the assessment of subsurface parameters in a hydro-geomechanical model, and to better estimate historical groundwater extractions in the Bandung groundwater basin where information regarding groundwater levels and groundwater use is scarce or unreliable. Given the paucity of comprehensive, spatially distributed groundwater data in the study area, such as limited hydraulic head measurements and uncertain groundwater pumping rates, the primary objective of the model calibration phase was to estimate the historical groundwater extraction that have contributed to the observed high rates of land subsidence within the basin. This research holds significant implications as the availability of high-quality groundwater resources decrease due to escalating groundwater extraction globally, particularly in arid agricultural and urban regions (Lall et al., 2020). A constraint in groundwater stress assessments is the acquisition of precise, concurrent groundwater extraction volumes at suitable temporal and spatial scales. Groundwater usage estimates are frequently characterized by uncertainty due to the absence of organized monitoring or data collection on pumping activities in many regions (Lall et al., 2020). The scarcity of comprehensive data to quantify these trends underscores the need for investigations, as exemplified by the present study.

The developed hydro-geomechanical model effectively simulates the temporal evolution of groundwater levels and the resulting vertical ground displacement within the Bandung groundwater basin. Our findings demonstrate a strong correlation between the locations of widespread groundwater drawdown centres and areas with higher industrial activity (Fig. 10, confirming the significant impact of groundwater extraction on land subsidence. The model highlights the predominant role of the deep aquifer unit in driving subsidence, which is vulnerable to compaction due to the presence of thick, compressible alluvial deposits that form the basin and triggered by the high rates of groundwater extraction in this unit. While the shallow aquifer unit is less susceptible to subsidence due to its unconfined nature and potential for recharge, the deeper aquifer unit's confined characteristics and greater extraction rates contribute significantly to the observed land subsidence. In line with previous studies (Khakim et al., 2014, Widodo et al., 2021), we demonstrate that the basin's lithological composition plays a significant role in its susceptibility to land subsidence due to the presence of highly compressible deposits, while the high degree of aquifer compaction is controlled by excessive industrial groundwater extraction.

The simulated groundwater head contours align with expectations, showing gentler gradients in the shallow aquifer unit compared to the deeper aquifer unit. This is attributed to lower pumping rates associated with domestic groundwater extraction and the influence of groundwater recharge in the shallower unit. However, both aquifer units exhibit widespread cones of depression in the western portion of the basin, reflecting the region's heavy reliance on groundwater for residential and industrial purposes. To the west of the basin, the widespread cone of depression observed in both aquifer units (Fig. 10) is located in a region dominated by residential

buildings and numerous industrial complexes, highlighting the large, mixed dependence of groundwater in this region of Bandung city. However, the highest rates of land subsidence are located in areas of spatially concentrated industrial complexes which have higher volumes of groundwater extraction (Fig. 12) and exhibit more significant drawdowns within the deep aquifer unit compared to other urbanised areas (Fig. 9 & 10). This suggests that the majority of the ground subsidence can be explained by the lowering of the water table, particularly in areas where many industrial buildings are present, due to the compound effects of multiple sources of groundwater extraction from the deep aquifer for industrial purposes. These findings confirm that the high rates of land subsidence in the Bandung groundwater basin are predominantly caused by groundwater depletion of the deep confined aquifer and corroborate with previous investigations which suggested that industrial water usage predominantly contributes to local subsidence (Chaussard et al., 2013) and have also attributed higher rates of land subsidence to areas with a higher percentage of industrial land cover (Widodo et al., 2021).

Two additional subsidence bowls are observed in the eastern portion of the basin, which correspond with presence of two groundwater cones of depression within the deeper aquifer unit (Fig. 10). These subsidence zones are smaller than the large subsidence feature simulated in western Bandung, both in terms of spatial extent and rates of subsidence (Fig. 8). In both cases, the centre of the subsidence bowl coincides with the occurrence of an industrial complex, implying that the subsidence is largely due to groundwater pumping from the deeper, confined aquifer for industrial purposes. However, in this region, the unconfined shallow aquifer is less exploited compared to western Bandung since this area is mostly covered by rice fields with few residential areas. Notably, groundwater is minimally used for irrigation purposes in the Bandung groundwater basin (Ohgaki et al., 2006), and therefore regions of agricultural land cover are devoid of groundwater extraction in the model. The lack of residential groundwater exploitation along with a lower density of industrial buildings, and thus less water extracted from the aquifer system overall, could explain the more localised and less severe occurrence of subsidence in eastern Bandung compared to the widespread and fast subsidence rates observed in the western portion of the basin.

As described in Section 2.3, groundwater-usage estimates in the Bandung groundwater basin are highly uncertain, which is reflected in the wide range of possible groundwater use volumes simulated in our model (Fig. 11). Taufiq et al. (2018) using a simple hydrogeological model suggested that the annual simulated industrial groundwater pumping volume reached a maximum value in 1995 of approximately 100 million m^3/yr (Mm^3/yr). In recent years, between 2010 and 2015, they suggest pumping reached a relatively constant annual extraction rate of 255 Mm^3/yr, mostly from the deeper aquifer. However, we found that in order for the model to simulate the high subsidence rates observed in recent years (up to −18.7 cm/yr; (Rygus et al., 2023)), the aquifer units needed to be undergoing inelastic compaction, implying that the groundwater level was declining below the pre-consolidation level. For this to occur, the groundwater pumping rates from the confined aquifer needed to continually increase by about 1 % in the last decade, eventually reaching a maximum annual pumping volume of 381 Mm^3 (98–1207 Mm^3, 95 % range). These findings are in accordance with recent modelling activities in the Bandung groundwater basin, which investigated the aquifer interaction between the unconfined and confined aquifers using tracer tests and found that groundwater extraction rates were between 202.9 Mm^3/yr to 322 Mm^3/year over 2005–2018 (Rusli et al., 2023b).

The recent spatial distribution of groundwater extraction in the Bandung groundwater basin, as revealed by this study (Fig. 12), provides valuable insights into the areas experiencing the most pressure on the groundwater resource. The concentration of high extraction rates within the deeper aquifer in the central-western portion of the basin, particularly in the vicinity of multiple industrial complexes (Fig. 1), highlights the excessive pumping of groundwater in this location to meet the demands of industries, which has resulted in a decline in groundwater levels (Fig. 10). This depletion suggests that there may be insufficient regulations or enforcement mechanisms to control groundwater extraction, allowing industries to extract water without considering the long-term sustainability of the resource.

The spatial distribution of the domestic groundwater use from the upper aquifer unit (Fig. 12) is mostly uniformly distributed throughout the urban area within the basin centre (indicated in Fig. 1). Notably, the cone of depression observed in the upper aquifer closely resembles the spatial pattern of the deeper aquifer unit (Fig. 10), deviating from the expected distribution based solely on domestic groundwater usage. This suggests potential hydraulic interactions between the two aquifers, a finding supported by previous research by Rusli et al. (2023b). In the region where groundwater levels are at their lowest in both aquifer units, characterized by intensive deep groundwater abstraction, a downward movement of groundwater is experienced (Rusli et al., 2023b). The substantial and concentrated industrial extraction from the deep aquifer significantly reduces confined groundwater pressures, steepens the hydraulic gradient between the aquifers, and consequently forces groundwater from the upper aquifer to flow downward. This downward movement of water could potentially lead to reduced water availability in the upper aquifer, thereby creating challenges for domestic water supply, especially during dry seasons or periods of peak demand.

Our model simulates that increasing groundwater extraction, particularly for industrial use, is driving groundwater storage depletion in the Bandung groundwater basin (Fig. 13). These findings align with a previous study that utilized GRACE satellite measurements and model-simulated water storage change estimates, revealing a sustained decline in aquifer storage from 2005 to 2019 due to escalating groundwater extraction rates (Rusli et al., 2023b). To capture the hydro-mechanical coupling between pore-fluid pressure and aquifer-system compaction in fine-grained sediments, we incorporated the CSUB package into our model. This allowed us to assess groundwater storage changes resulting from the depressurization of interbeds (Hughes et al., 2022). Our model simulates that the majority of storage depletion in the Bandung groundwater basin arises from prolonged declines in groundwater levels. In areas where the groundwater level decline and areal extent are substantial, a significant portion of the water supplied to wells has been sourced from groundwater released from storage in the fine-grained interbeds or confining units, which has led to inelastic compaction (Poland, 1984). Our model simulation shows that long-term groundwater-level declines have resulted primarily in inelastic compaction, driven by increasingly large amounts of water extracted from the deeper, confined aquifer unit, with only a small

percentage of water derived from elastic compaction during the model period (Fig. 13). Therefore, the majority of water released from aquifer storage constitutes a one-time extraction of stored water which has resulted in a substantial irreversible decline in aquifer-system storage capacity (Riley 1998; Sneed and Galloway 2000). Along with the increasing trend of groundwater extraction for both domestic and industrial use (Fig. 11), the corresponding negative trend of permanent groundwater storage loss (Fig. 13) highlights the unsustainable groundwater management policy in the Bandung groundwater basin.

While InSAR offers a measurement of total land surface vertical displacement, it is unable to differentiate between the contributions of individual subsurface units to this deformation. In contrast, the hydro-geomechanical model employed in this study can simulate the deformation of each layer, providing a detailed analysis of the factors influencing overall surface deformation (Fig. 10). Calibration of model parameters, including compaction coefficients, hydraulic properties, and groundwater extraction rates, was essential to ensure alignment between simulated and observed surface deformation, as derived from InSAR. Although historical groundwater head data for calibration was limited to the deeper aquifer unit (model layer 3), the predominant groundwater users in the region are industries, necessitating a history-matching approach that focused on aligning overall InSAR-derived subsidence with the response of the deeper aquifer's groundwater head. This is supported by the model output which revealed that the fine-grained interbeds within the deeper aquifer unit accounted for most of the total compaction (68–72 %; Table 2) simulated for the period 1950–2020. To further enhance the model's robustness and accuracy, incorporating measurements of hydraulic head from the upper aquifer into the model history-matching would be advantageous; however, this data is currently unavailable. Establishing a comprehensive groundwater monitoring network in the Bandung groundwater basin would enable the integration of further data into the model, enhancing its predictive capabilities and facilitating more effective groundwater management and land subsidence mitigation in the region.

A forecast period was included in the model to assess the impact of future groundwater extraction in the Bandung groundwater basin until 2050 under sustained, increased, and decreased industrial pumping scenarios. A limitation of the predictive model is that we assumed that the spatial distribution of the future pumping remains the same as that in 2020. Therefore, the expansion of groundwater pumping as a result of urban growth or land use change is not considered. This is observed in Fig. 14 which depicts the forecasted cumulative subsidence over the various pumping forecasts. While the magnitude of additional subsidence varies, the spatial distribution of subsidence is similar when comparing the three different scenarios. The subsidence hotspot in western Bandung, along with the two eastern subsidence bowls, are simulated in all scenarios. Loss of aquifer storage capacity due to land subsidence cannot be avoided in any scenario, and unsurprisingly, the scenario simulating increased industrial pumping resulted in the greatest loss of aquifer storage. The discovery that the model simulates an additional irreversible loss of aquifer storage capacity of 9.2 km^3 by 2050 even with a reduction of expected industrial groundwater extraction by 30 % (Fig. 14) highlights the need to address unsustainable groundwater management in the basin to prevent additional land subsidence and storage loss. The 20-year model projection period offers a starting point for simulating various future scenarios of groundwater usage. These simulations can be refined to reflect more accurate estimates of groundwater utilisation, considering new groundwater developments or planned groundwater replenishment activities.

Our findings highlight the importance of sustainable groundwater management in the Bandung basin. Excessive groundwater extraction, the primary cause of land subsidence in the region, is anticipated to be exacerbated by increasing demands on water resources. In Bandung, projected increases in temperature and decreases in rainfall are likely to reduce groundwater recharge in the coming decades (Shrestha et al., 2018). The confluence of reduced aquifer replenishment and ongoing unsustainable groundwater extraction due to urbanization and economic development could exacerbate the existing imbalance between aquifer replenishment and withdrawal, leading to accelerated groundwater depletion and associated land subsidence. To mitigate these impacts, several strategies can be implemented, including those proposed by Satriyo et al. (2024): controlling groundwater use through vulnerability zoning, utilizing surface water to reduce reliance on groundwater, increasing groundwater recharge via injection wells, and implementing spatial planning that accommodates subsidence issues. Additionally, establishing robust monitoring systems for land subsidence and groundwater levels is essential for tracking changes and adapting management practices effectively.

5. Conclusion

Groundwater extraction-induced subsidence is a global threat that poses significant socio-economic challenges to human populations, infrastructure, and ecosystems.

In this work a hydro-geomechanical was developed for the Bandung groundwater basin aquifer system to assess the relationship between the groundwater withdrawal and subsidence, as well as to constrain historical groundwater pumping rates, and provide insights for sustainable groundwater management. The integration of InSAR data was key to address the lack of hydrogeological and historical actual abstraction data.

The model shows that extensive and increasing groundwater withdrawal from the aquifer system since 1950 has had a significant impact on potentiometric heads and as well as been the primary cause of land subsidence. For instance, the simulated water budget indicates that 97 % of the total groundwater withdrawn from the aquifer is originating from permanent compaction and therefore from an irreversible loss of groundwater storage. Groundwater extraction from 1950 to 2020 has also resulted in an average of 4 m of ground subsidence in the Bandung groundwater basin. By using the model to assess the impact of different groundwater pumping scenarios, it was forecasted that "business-as-usual" groundwater extraction from 2020 to 2050 will lead to additional land subsidence of up to 5.6 m ($\pm$ 1.1 m) in central-west Bandung.

Furthermore, the model shows that groundwater extraction has led to irreversible changes in the aquifer system such as a loss of aquifer storage capacity of 7.2 km^3. This volume is projected to nearly double by 2050 at the current rate of groundwater abstraction. With a decrease of 30 % in groundwater withdrawal used for industrial activities by 2050, the land is expected to further subside up to

5.1 m (± 1.0 m) in western Bandung while the eastern area will incur up to 1.9 m (± 0.6 m) of extra subsidence. Compared to the "business-as-usual" scenario, the additional volume loss of aquifer storage capacity can be reduced by up to 17 %. With a 30 % increase in groundwater extraction by 2050, the model predicts further land subsidence, up to 6.3 m (± 1.2 m) in western Bandung, and an additional loss of aquifer storage capacity 18 % greater than the "business-as-usual" scenario.

This study demonstrates the benefit of integrating InSAR satellite data into the traditional groundwater modelling framework to develop a more robust tool for groundwater resource management in data-scarce aquifer systems subject to extensive abstraction and consequential land subsidence. Results suggest that improving the management of industrial groundwater use in the Bandung area could prevent further subsidence and help achieve a more sustainable use of the resource. Mitigation measures could include defining and (re-)allocating groundwater property rights, regulating its use, regular groundwater monitoring initiatives, or implementing wide-scale artificial recharge to recover groundwater levels that have declined due to unsustainable extraction.

CRediT authorship contribution statement

Marco Bianchi: Writing – review & editing, Supervision, Formal analysis. **Alessandro Novellino:** Writing – review & editing, Supervision, Resources, Project administration, Funding acquisition. **Ekbal Hussain:** Writing – review & editing, Supervision, Data curation. **Ahmad Taufiq:** Writing – review & editing, Data curation. **Michelle Rygus:** Writing – original draft, Visualization, Methodology, Investigation, Formal analysis, Data curation, Conceptualization. **Claudia Meisina:** Writing – review & editing, Supervision. **Steven Reinaldo Rusli:** Writing – review & editing, Data curation. **Dwi Sarah:** Writing – review & editing, Data curation.

Declaration of Competing Interest

The authors declare that they have no known competing financial interests or personal relationships that could have appeared to influence the work reported in this paper.

Acknowledgments

This study was carried out by M. Rygus in the framework of her PhD project at the University of Pavia and during her research visit at the British Geological Survey (BGS) in October to December 2022, under the supervision of M. Bianchi, A. Novellino, E. Hussain, and C. Meisina. The research was part of the BGS International NC programme 'Geoscience to tackle Global Environmental Challenges', NERC reference NE/X006255/1. M. Bianchi, A. Novellino, and E. Hussain publish with permission from the Executive Director of the British Geological Survey.

Appendix A. Supporting information

Supplementary data associated with this article can be found in the online version at doi:10.1016/j.ejrh.2024.102129.

Data availability

Data will be made available on request.

References

Abidin, H.Z., Andreas, H., Gamal, M., et al., 2008. Land subsidence characteristics of the Bandung Basin, Indonesia, as estimated from GPS and InSAR, 2, 167–177. https://doi.org/10.1515/JAG.2008.019.

Abidin, H.Z., Gumilar, I., Andreas, H., et al., 2013. On causes and impacts of land subsidence in Bandung Basin, Indonesia. Environ. Earth Sci. 68, 1545–1553. https://doi.org/10.1007/s12665-012-1848-z.

Anderson, M., Woessner, W., Hunt, R., 2015. Appl. Ground Water Model.: Simul. Flow. Advective Transp.

Bateson, L., Novellino, A., Hussain, E., Arnhardt, R., Nguyen, H.K., 2023. Urban development induced subsidence in deltaic environments: A case study in Hanoi, Vietnam. Int. J. Appl. Earth Obs. Geoinf. 125, 103585.

Berardino, P., Fornaro, G., Lanari, R., Sansosti, E., 2002. A new algorithm for surface deformation monitoring based on small baseline differential SAR interferograms. IEEE Trans. Geosci. Remote Sens 40, 2375–2383. https://doi.org/10.1109/TGRS.2002.803792.

Bockstiegel, M., Richard-Cerda, J.C., Muñoz-Vega, E., et al., 2023. Simulation of present and future land subsidence in the Rafsanjan plain, Iran, due to groundwater overexploitation using numerical modeling and InSAR data analysis. Hydrogeol. J. https://doi.org/10.1007/s10040-023-02657-y.

Bradski, G., 2000. Open. Libr.

Burbey, T.J., Zhang, M., 2015. Inverse modeling using PS-InSAR for improved calibration of hydraulic parameters and prediction of future subsidence for Las Vegas Valley, USA. : Proc. Int. Assoc. Hydrol. Sci. 411–416.

Calderhead, A.I., Therrien, R., Rivera, A., et al., 2011. Simulating pumping-induced regional land subsidence with the use of InSAR and field data in the Toluca Valley, Mexico. Adv. Water Resour. 34, 83–97. https://doi.org/10.1016/j.advwatres.2010.09.017.

Ceccatelli, M., Del Soldato, M., Solari, L., et al., 2021. Numerical modelling of land subsidence related to groundwater withdrawal in the Firenze-Prato-Pistoia basin (central Italy). Hydrogeol. J. 29, 629–649. https://doi.org/10.1007/s10040-020-02255-2.

Chaussard, E., Amelung, F., Abidin, H., Hong, S.-H., 2013. Sinking cities in Indonesia: ALOS PALSAR detects rapid subsidence due to groundwater and gas extraction. Remote Sens Environ. 128, 150–161. https://doi.org/10.1016/j.rse.2012.10.015.

Chowdhury, F., Gong, J., Rau, G.C., Timms, W.A., 2022. Multifactor analysis of specific storage estimates and implications for transient groundwater modelling. Hydrogeol. J. 30, 2183–2204. https://doi.org/10.1007/s10040-022-02535-z.
Deutscher Wetterdienst, 2022a. Index /climate_environment/GPCC/ https://opendata.dwd.de/climate_environment/GPCC/. Accessed 2 Jan 2024.
Doherty, J., 2003. Ground water model calibration using pilot points and regularization. Ground Water 41, 170–177. https://doi.org/10.1111/j.1745-6584.2003.tb02580.x.
Doherty, J., Simmons, C.T., 2013. Groundwater modelling in decision support: reflections on a unified conceptual framework. Hydrogeol. J. 21, 1531–1537. https://doi.org/10.1007/s10040-013-1027-7.
Du, Z., Ge, L., Ng, A.H.-M., et al., 2018. Correlating the subsidence pattern and land use in Bandung, Indonesia with both Sentinel-1/2 and ALOS-2 satellite images. Int J. Appl. Earth Obs. Geoinf. 67, 54–68. https://doi.org/10.1016/j.jag.2018.01.001.
Ezquerro, P., Guardiola-Albert, C., Herrera, G., et al., 2017. Groundwater and Subsidence Modeling Combining Geological and Multi-Satellite SAR Data over the Alto Guadalentín Aquifer (SE Spain). Geofluids 2017, e1359325. https://doi.org/10.1155/2017/1359325.
Ferretti, A., Prati, C., Rocca, F., 2001. Permanent scatterers in SAR interferometry. IEEE Trans. Geosci. Remote Sens 39, 8–20. https://doi.org/10.1109/36.898661.
Funk, C., Peterson, P., Landsfeld, M., et al., 2015. The climate hazards infrared precipitation with stations—a new environmental record for monitoring extremes. Sci. Data 2, 150066. https://doi.org/10.1038/sdata.2015.66.
Galloway, D.L., Burbey, T.J., 2011. Review: Regional land subsidence accompanying groundwater extraction. Hydrogeol. J. 19, 1459–1486. https://doi.org/10.1007/s10040-011-0775-5.
Gleeson, T., Wada, Y., Bierkens, M.F.P., van Beek, L.P.H., 2012. Water balance of global aquifers revealed by groundwater footprint. Nature 488, 197–200. https://doi.org/10.1038/nature11295.
Gumilar, I., Sidiq, T., Meilano, I., et al., 2021. Extensive Investigation of the Land Subsidence Impressions on Gedebage District, Bandung, Indonesia. IOP Conf. Ser. Earth Environ. Sci. 873, 012044. https://doi.org/10.1088/1755-1315/873/1/012044.
Guzy, A., Malinowska, A.A., 2020. State of the Art and Recent Advancements in the Modelling of Land Subsidence Induced by Groundwater Withdrawal. Water 12, 2051. https://doi.org/10.3390/w12072051.
Herrera-García, G., Ezquerro, P., Tomás, R., et al., 2021. Mapping the global threat of land subsidence. Science 371, 34–36. https://doi.org/10.1126/science.abb8549.
Hoffmann, J., Zebker, H.A., Galloway, D.L., Amelung, F., 2001. Seasonal subsidence and rebound in Las Vegas Valley, Nevada, observed by Synthetic Aperture Radar Interferometry. Water Resour. Res 37, 1551–1566. https://doi.org/10.1029/2000WR900404.
Holzer, T.L., Pampeyan, E.H., 1981. Earth fissures and localized differential subsidence. Water Resour. Res 17, 223–227. https://doi.org/10.1029/WR017i001p00223.
Hughes, J.D., Leake, S.A., Galloway, D.L., White, J.T., 2022. Documentation for the Skeletal Storage, Compaction, and Subsidence (CSUB) Package of MODFLOW 6. U. S. Geological Survey.
Hunt, R.J., White, J.T., Duncan, L.L., et al., 2021. Evaluating Lower Computational Burden Approaches for Calibration of Large Environmental Models. Groundwater 59, 788–798. https://doi.org/10.1111/gwat.13106.
Hunt, R.J., Zheng, C., 2012. The Current State of Modeling. Groundwater 50, 330–333. https://doi.org/10.1111/j.1745-6584.2012.00936.x.
Hutasoit, L., 2009. Kondisi Permukaan Air Tanah dengan dan tanpa peresapan buatan di daerah Bandung: Hasil Simulasi Numerik. Indones. J. Geosci. https://doi.org/10.17014/ijog.vol4no3.20093.
Khakim, M.Y.N., Tsuji, T., Matsuoka, T., 2014. Lithology-controlled subsidence and seasonal aquifer response in the Bandung basin, Indonesia, observed by synthetic aperture radar interferometry. Int J. Appl. Earth Obs. Geoinf. 32, 199–207. https://doi.org/10.1016/j.jag.2014.04.012.
Lall, U., Josset, L., Russo, T., 2020. A Snapshot of the World's Groundwater Challenges. Annu. Rev. Environ. Resour. 45, 171–194. https://doi.org/10.1146/annurev-environ-102017-025800.
Langevin, C.D., Hughes, J.D., Banta, E.R., et al., 2017. Documentation for the MODFLOW 6 Groundwater Flow Model. U. S. Geol. Surv.
Li, J., Zhu, L., Gong, H., et al., 2022. Unraveling elastic and inelastic storage of aquifer systems by integrating fast independent component analysis and a variable preconsolidation head decomposition method. J. Hydrol. 606, 127420. https://doi.org/10.1016/j.jhydrol.2021.127420.
Lo, W., Purnomo, S.N., Dewanto, B.G., et al., 2022. Integration of Numerical Models and InSAR Techniques to Assess Land Subsidence Due to Excessive Groundwater Abstraction in the Coastal and Lowland Regions of Semarang City. Water 14, 201. https://doi.org/10.3390/w14020201.
Meade, R.H., 1964. Removal of water and rearrangement of particles during the compaction of clayey sediments - review. Prof. Pap. https://doi.org/10.3133/pp497B.
OECD, 2018. Active with Indonesia. Available at: https://www.oecd.org/indonesia/Active-with-Indonesia.pdf [accessed on 2/4/2024]. Available at: https://www.oecd.org/indonesia/Active-with-Indonesia.pdf [accessed on 2/4/2024].
Ohenhen, L.O., Shirzaei, M., Ojha, C., Sherpa, S.F., Nicholls, R.J., 2024. Disappearing cities on US coasts. Nature 627 (8002), 108–115. https://doi.org/10.1038/s41586-024-07038-3.
Orellana, F., Rivera, D., Montalva, G., Arumi, J.L., 2023. InSAR-Based Early Warning Monitoring Framework to Assess Aquifer Deterioration. Remote Sens 15, 1786. https://doi.org/10.3390/rs15071786.
Poland, J.F., 1984. Guideb. Stud. Land Subsid. Ground-Water withdrawal.
Prasetyo, Y., Tetuko, S.S., Ismullah, I.H., et al., 2013. Data optimalization in permanent scatterer interferometric synthetic aperture radar (PS-INSAR) technique for land subsidence estimation. 34th Asian Conf. Remote Sens 1064–1072.
Rahiem, M.A., 2020. Indonesia. Hydrogeol. Inf. Bdg. Basin https://malikarrahiem.shinyapps.io/BandungBasin/ (2020).
Riley, F.S., 1969b. Analysis of borehole extensometer data from central California - UNESCO Digital Library. In: Land Subsidence. nt. Assoc. Sci. Hydrol. Publ, pp. 423–431.
Rose, H.E., 1945. An Investigation into the Laws of Flow of Fluids through Beds of Granular Materials. Proc. Inst. Mech. Eng. 153, 141–148. https://doi.org/10.1243/PIME_PROC_1945_153_018_02.
Rusli, S.R., Bense, V.F., Taufiq, A., Weerts, A.H., 2023a. Quantifying basin-scale changes in groundwater storage using GRACE and one-way coupled hydrological and groundwater flow model in the data-scarce Bandung groundwater Basin, Indonesia. Ground Sustain Dev. 22, 100953. https://doi.org/10.1016/j.gsd.2023.100953.
Rusli, S.R., Weerts, A.H., Mustafa, S.M.T., et al., 2023b. Quantifying aquifer interaction using numerical groundwater flow model evaluated by environmental water tracer data: Application to the data-scarce area of the Bandung groundwater basin, West Java, Indonesia. J. Hydrol. Reg. Stud. 50, 101585. https://doi.org/10.1016/j.ejrh.2023.101585.
Rusli, S.R., Weerts, A.H., Taufiq, A., Bense, V.F., 2021. Estimating water balance components and their uncertainty bounds in highly groundwater-dependent and data-scarce area: An example for the Upper Citarum basin. J. Hydrol. Reg. Stud. 37, 100911. https://doi.org/10.1016/j.ejrh.2021.100911.
Rygus, M., Novellino, A., Hussain, E., et al., 2023. A Clustering Approach for the Analysis of InSAR Time Series: Application to the Bandung Basin (Indonesia). Remote Sens 15, 3776. https://doi.org/10.3390/rs15153776.
Sadeghi, Z., Wright, T.J., Hooper, A.J., et al., 2021. Benchmarking and inter-comparison of Sentinel-1 InSAR velocities and time series. Remote Sens Environ. 256, 112306. https://doi.org/10.1016/j.rse.2021.112306.
Satriyo, N.A., Mulyono, A., Wibawa, S., Yuliyanti, A., Sari, A.M., Putra, Moch H.Z., Arfiyansyah, K., 2024. The review of the geological disaster of Bandung Basin subsurface: perspective from geological approach. Geol., Ecol., Landsc. 1–19. https://doi.org/10.1080/24749508.2024.2359781.
Shrestha, S., Hoang, N., Shrestha, P., Bhatta, B., 2018. Climate change impact on groundwater recharge and suggested adaptation strategies for selected Asian cities. APN Sci. Bull. 8 (1). https://doi.org/10.30852/sb.2018.499.
Siswanto, S.Y., Francés, F., 2019. How land use/land cover changes can affect water, flooding and sedimentation in a tropical watershed: a case study using distributed modeling in the Upper Citarum watershed, Indonesia. Environ. Earth Sci. 78, 550. https://doi.org/10.1007/s12665-019-8561-0.
Sneed, M., 2001. Hydraulic and mechanical properties affecting ground-water flow and aquifer-system compaction. San Joaquin Valley, California. https://doi.org/10.3133/ofr0135.

Sri Sumantyo, J.T., Shimada, M., Mathieu, P.-P., Abidin, H.Z., 2012. Long-Term Consecutive DInSAR for Volume Change Estimation of Land Deformation. IEEE Trans. Geosci. Remote Sens 50, 259–270. https://doi.org/10.1109/TGRS.2011.2160455.

Taufiq, A., 2010. Land subsidence study for Bandung and surrounding areas (case study area: Dayeuhkolot, Rancaekek and Cimahi) (in Indonesian). MSc Thesis, Bandung Institute of Technology (ITB). Bandung, Indonesia.

Taufiq, A., Hosono, T., Ide, K., et al., 2018. Impact of excessive groundwater pumping on rejuvenation processes in the Bandung basin (Indonesia) as determined by hydrogeochemistry and modeling. Hydrogeol. J. 26, 1263–1279. https://doi.org/10.1007/s10040-017-1696-8.

Terzaghi, K., 1926. Principles of Soil Mechanics: A Summary of Experimental Studies of Clay and Sand. McGraw-Hill.

Tirtomihardjo, H., 2016. Chapter 10 - Groundwater Environment in Bandung, Indonesia. In: Shrestha, S., Pandey, V.P., Shivakoti, B.R., Thatikonda, S. (Eds.), Groundwater Environment in Asian Cities. Butterworth-Heinemann, pp. 193–228.

White, J.T., 2018. A model-independent iterative ensemble smoother for efficient history-matching and uncertainty quantification in very high dimensions. Environ. Model Softw. 109, 191–201. https://doi.org/10.1016/j.envsoft.2018.06.009.

White, J.T., Fienen, M.N., Doherty, J.E., 2016. A python framework for environmental model uncertainty analysis. Environ. Model Softw. 85, 217–228. https://doi.org/10.1016/j.envsoft.2016.08.017.

Widodo, J., Naryanto, H.S., Wisyanto, Hidayat, N., Putra, A.P., Izumi, Y., Perissin, D., Sri Sumantyo, J.T., 2021. Land Subsidence Assessment of Bandung City, Indonesia in Geological Perspective, Based on Interferometric SAR Using C-band Data. In: Photonics & Electromagnetics Research Symposium (PIERS), 2021. Hangzhou, China, pp. 2377–2381. https://doi.org/10.1109/PIERS53385.2021.9694892.